# aneeh_thesis_final.pdf

Delhi Technological University

## Document Details

**Submission ID**

**trn:oid:::27535:98927886**

**Submission Date**

**Jun 2, 2025, 11:45 AM GMT+5:30**

**Download Date**

**Jun 2, 2025, 11:47 AM GMT+5:30**

**File Name**

**aneeh_thesis_final.pdf**

**File Size**

**2.6 MB**

**73 Pages**

**18,012 Words**

**97,117 Characters**

# 15% Overall Similarity

The combined total of all matches, including overlapping sources, for each database.

## Filtered from the Report

- Bibliography
- Quoted Text
- Cited Text
- Small Matches (less than 10 words)

## Match Groups

**176** Not Cited or Quoted 15%
Matches with neither in-text citation nor quotation marks

**0** Missing Quotations 0%
Matches that are still very similar to source material

**0** Missing Citation 0%
Matches that have quotation marks, but no in-text citation

**0** Cited and Quoted 0%
Matches with in-text citation present, but no quotation marks

## Top Sources

8%  🌐 Internet sources

9%  📖 Publications

8%  👤 Submitted works (Student Papers)

## Integrity Flags

**0 Integrity Flags for Review**

No suspicious text manipulations found.

Our system's algorithms look deeply at a document for any inconsistencies that would set it apart from a normal submission. If we notice something strange, we flag it for you to review.

A Flag is not necessarily an indicator of a problem. However, we'd recommend you focus your attention there for further review.

## Match Groups

**176** Not Cited or Quoted 15%
Matches with neither in-text citation nor quotation marks

**0** Missing Quotations 0%
Matches that are still very similar to source material

**0** Missing Citation 0%
Matches that have quotation marks, but no in-text citation

**0** Cited and Quoted 0%
Matches with in-text citation present, but no quotation marks

## Top Sources

8%  🌐 Internet sources

9%  📖 Publications

8%  👤 Submitted works (Student Papers)

## Top Sources

The sources with the highest number of matches within the submission. Overlapping sources will not be displayed.

| 1 | Internet | | |
|---|---|---|---|
| www.researchgate.net | | | 2% |

| 2 | Submitted works | | |
|---|---|---|---|
| Delhi Technological University on 2024-05-23 | | | <1% |

| 3 | Publication | | |
|---|---|---|---|
| Damith Buddika Wickramasinghe Abeywardana, Pablo Acuna, Branislav Hredzak,... | | | <1% |

| 4 | Publication | | |
|---|---|---|---|
| Monteiro, Vitor, Gabriel Pinto, and Joao Afonso. "Operation Modes for the Electric... | | | <1% |

| 5 | Submitted works | | |
|---|---|---|---|
| dtusimilarity on 2024-05-29 | | | <1% |

| 6 | Internet | | |
|---|---|---|---|
| www.mpce.info | | | <1% |

| 7 | Internet | | |
|---|---|---|---|
| www.mdpi.com | | | <1% |

| 8 | Internet | | |
|---|---|---|---|
| dspace.dtu.ac.in:8080 | | | <1% |

| 9 | Publication | | |
|---|---|---|---|
| Bhushan P. Mokal, K. Vadirajacharya. "Extensive modeling of DC-DC cuk converte... | | | <1% |

| 10 | Internet | | |
|---|---|---|---|
| www.scielo.org.mx | | | <1% |

**11** Publication

Praanshu Srijan Shandilya, Ashutosh Gupta, Dheeraj Joshi. "Voltage and Current ...        <1%

**12** Publication

Debasish Mishra, Bhim Singh, B.K. Panigrahi. "Implementation of a Robust PMAE ...        <1%

**13** Publication

Abed Kazemtarghi, Saikat Dey, Ayan Mallik. "Optimal Utilization of Bidirectional E...        <1%

**14** Submitted works

Gitam University on 2024-11-04        <1%

**15** Submitted works

University Of Tasmania on 2011-06-06        <1%

**16** Internet

ebin.pub        <1%

**17** Publication

Krishnan K Gokul, Babu P Emmanuel, S Ashok, S Kumaravel. "Design and control ...        <1%

**18** Internet

discol.umk.edu.my        <1%

**19** Publication

Utsav Sharma, Bhim Singh. "A Non-isolated Onboard Charger for Electric Vehicle"...        <1%

**20** Submitted works

Anna University on 2024-03-16        <1%

**21** Internet

dc.uwm.edu        <1%

**22** Internet

discovery.researcher.life        <1%

**23** Publication

"Energy and Environmental Aspects of Emerging Technologies for Smart Grid", Sp...        <1%

**24** Publication

Singh, Mukhtiar. "Adaptive network-based fuzzy inference systems for sensorless...        <1%

| 25 | Internet | |
|----|----------|--|
| ijirset.com | | <1% |

| 26 | Internet | |
|----|----------|--|
| www.coursehero.com | | <1% |

| 27 | Submitted works | |
|----|----------|--|
| IIT Delhi on 2016-10-11 | | <1% |

| 28 | Submitted works | |
|----|----------|--|
| University of Teesside on 2025-01-06 | | <1% |

| 29 | Publication | |
|----|----------|--|
| Weearsinghe, Saranga, Duleepa J. Thrimawithana, and Udaya K. Madawala. "Mod... | | <1% |

| 30 | Submitted works | |
|----|----------|--|
| University of Leeds on 2015-04-23 | | <1% |

| 31 | Submitted works | |
|----|----------|--|
| Visvesvaraya Technological University, Belagavi on 2022-10-20 | | <1% |

| 32 | Internet | |
|----|----------|--|
| dtu.ac.in | | <1% |

| 33 | Publication | |
|----|----------|--|
| Kanimozhi K, K. K. Prabhakaran, Nagendrappa Harischandrappa, B. Venkatesaper... | | <1% |

| 34 | Submitted works | |
|----|----------|--|
| PEC University of Technology on 2020-06-27 | | <1% |

| 35 | Publication | |
|----|----------|--|
| Shailendra Kumar, Tapesh Upadhyay, Om Hari Gupta. "Power Quality Improveme... | | <1% |

| 36 | Submitted works | |
|----|----------|--|
| De Montfort University on 2016-05-03 | | <1% |

| 37 | Submitted works | |
|----|----------|--|
| Indian Institute of Technology, Bombay on 2013-09-01 | | <1% |

| 38 | Submitted works | |
|----|----------|--|
| SASTRA University on 2013-04-25 | | <1% |

| 39 | Publication |
|----|----|

Saranga Weerasinghe, Udaya K. Madawala, Duleepa J. Thrimawithana. "A closed l...     <1%

| 40 | Submitted works |
|----|----|

Siddaganga Institute of Technology on 2019-05-11     <1%

| 41 | Publication |
|----|----|

Zhigang Zhang, Bin Liu, Shaojian Song. "Power Decoupling Control for V2G/G2V/P...     <1%

| 42 | Submitted works |
|----|----|

University of Newcastle upon Tyne on 2015-08-26     <1%

| 43 | Publication |
|----|----|

Zgheib, Rawad, Kamal Al-Haddad, and Innocent Kamwa. "V2G, G2V and active filt...     <1%

| 44 | Publication |
|----|----|

Gautam Rituraj, Gautham Ram Chandra Mouli, Pavol Bauer. "A Comprehensive R...     <1%

| 45 | Publication |
|----|----|

Mohd Khalid, Furkan Ahmad, Bijaya Ketan Panigrahi, Luluwah Al-Fagih. "A compr...     <1%

| 46 | Publication |
|----|----|

M.C. Annamalai, N. Amutha prabha. "A comprehensive review on isolated and no...     <1%

| 47 | Publication |
|----|----|

Kai-Wei Hu, Pei-Hsun Yi, Chang-Ming Liaw. "An EV SRM Drive Powered by Battery/...     <1%

| 48 | Submitted works |
|----|----|

Port Jervis High School on 2023-12-12     <1%

| 49 | Submitted works |
|----|----|

University of Sheffield on 2014-06-13     <1%

| 50 | Submitted works |
|----|----|

University of Sheffield on 2018-05-04     <1%

| 51 | Internet |
|----|----|

www.iitrpr.ac.in     <1%

| 52 | Submitted works |
|----|----|

Thapar University, Patiala on 2024-12-27     <1%

| 53 | Submitted works | |
|---|---|---|
| Curtin University of Technology on 2017-08-01 | | <1% |

| 54 | Publication | |
|---|---|---|
| Singh, M., V. Khadkikar, and A. Chandra. "Grid synchronisation with harmonics an... | | <1% |

| 55 | Submitted works | |
|---|---|---|
| University of Derby on 2020-05-24 | | <1% |

| 56 | Publication | |
|---|---|---|
| Vaibhav Shah, Saifullah Payami. "Integrated Converter with G2V, V2G, and DC/V2... | | <1% |

| 57 | Internet | |
|---|---|---|
| repositories.lib.utexas.edu | | <1% |

| 58 | Internet | |
|---|---|---|
| research.aalto.fi | | <1% |

| 59 | Internet | |
|---|---|---|
| www.grafiati.com | | <1% |

| 60 | Submitted works | |
|---|---|---|
| Amrita Vishwa Vidyapeetham on 2020-02-25 | | <1% |

| 61 | Publication | |
|---|---|---|
| Mohamed Mezouari, Meriem Megrini, Ahmed Gaga. "High efficiency DC–DC conv... | | <1% |

| 62 | Publication | |
|---|---|---|
| Mohamed Y. Metwly, Mahmoud S. Abdel-Majeed, Ayman S. Abdel-Khalik, Ragi A. ... | | <1% |

| 63 | Publication | |
|---|---|---|
| Utsav Sharma, Bhim Singh. "Modified Deadbeat Predictive Current Control based ... | | <1% |

| 64 | Internet | |
|---|---|---|
| autodocbox.com | | <1% |

| 65 | Internet | |
|---|---|---|
| par.nsf.gov | | <1% |

| 66 | Internet | |
|---|---|---|
| techgdpr.com | | <1% |

| 67 | Internet | |
|----|----------|---|
| www.dspace.dtu.ac.in:8080 | | <1% |

| 68 | Internet | |
|----|----------|---|
| yorkspace.library.yorku.ca | | <1% |

| 69 | Publication | |
|----|-------------|---|
| "Recent Advances in Electrical and Information Technologies for Sustainable Dev... | | <1% |

| 70 | Publication | |
|----|-------------|---|
| Diksha Singh, Mukesh Maurya, M.V. Gururaj, Laxmidhar Behera. "A Unique Energ... | | <1% |

| 71 | Submitted works | |
|----|-----------------|---|
| IIT Delhi on 2015-02-11 | | <1% |

| 72 | Submitted works | |
|----|-----------------|---|
| Indian Institute of Technology Roorkee on 2024-02-29 | | <1% |

| 73 | Publication | |
|----|-------------|---|
| Lin, Ray-Lee, and Rui-Che Wang. "Non-inverting buck-boost power-factor-correcti... | | <1% |

| 74 | Submitted works | |
|----|-----------------|---|
| National Institute of Technology, Rourkela on 2015-05-09 | | <1% |

| 75 | Publication | |
|----|-------------|---|
| Saranga Weerasinghe, Udaya K. Madawala, Duleepa J. Thrimawithana. "A Matrix ... | | <1% |

| 76 | Submitted works | |
|----|-----------------|---|
| Singapore Institute of Technology on 2025-03-23 | | <1% |

| 77 | Publication | |
|----|-------------|---|
| Sudev V., Sindhu M.R.. "State-of-the-art and future trends in electric vehicle charg... | | <1% |

| 78 | Submitted works | |
|----|-----------------|---|
| Universiti Teknikal Malaysia Melaka on 2014-05-14 | | <1% |

| 79 | Submitted works | |
|----|-----------------|---|
| University of Edinburgh on 2011-04-20 | | <1% |

| 80 | Submitted works | |
|----|-----------------|---|
| University of Lancaster on 2023-03-23 | | <1% |

**81** Submitted works

University of Queensland on 2024-11-13   <1%

**82** Submitted works

University of Western Sydney on 2023-06-09   <1%

**83** Internet

research.vu.nl   <1%

**84** Internet

storage.googleapis.com   <1%

**85** Internet

www.scilit.net   <1%

**86** Submitted works

Amity University on 2016-08-23   <1%

**87** Submitted works

CSU Office of the Chancellor on 2018-07-10   <1%

**88** Submitted works

College of Engineering & Technology Bhubaneswar on 2020-07-15   <1%

**89** Submitted works

Concordia University on 2024-05-31   <1%

**90** Publication

Fang Lin Luo, Hong Ye. "Renewable Energy Systems - Advanced Conversion Techn...   <1%

**91** Publication

Gangavarapu Guru Kumar, Kumaravel Sundaramoorthy. "Dual-Input Nonisolated...   <1%

**92** Submitted works

Higher Education Commission Pakistan on 2017-11-28   <1%

**93** Submitted works

IIT Delhi on 2017-02-10   <1%

**94** Submitted works

Indian Institute of Technology on 2020-03-16   <1%

| 95 | Publication | |
|---|---|---|
| Khairy Sayed, Hossam Gabbar. "Electric Vehicle to Power Grid Integration Using T... | | <1% |

| 96 | Submitted works | |
|---|---|---|
| Liverpool John Moores University on 2024-04-13 | | <1% |

| 97 | Submitted works | |
|---|---|---|
| University of Greenwich on 2024-03-08 | | <1% |

| 98 | Submitted works | |
|---|---|---|
| University of Hertfordshire on 2024-01-08 | | <1% |

| 99 | Submitted works | |
|---|---|---|
| University of Hong Kong on 2018-08-28 | | <1% |

| 100 | Submitted works | |
|---|---|---|
| University of Leeds on 2018-08-28 | | <1% |

| 101 | Submitted works | |
|---|---|---|
| University of Newcastle upon Tyne on 2013-08-30 | | <1% |

| 102 | Submitted works | |
|---|---|---|
| University of Warwick on 2016-11-14 | | <1% |

| 103 | Submitted works | |
|---|---|---|
| University of Western Sydney on 2023-02-03 | | <1% |

| 104 | Internet | |
|---|---|---|
| html.pdfcookie.com | | <1% |

| 105 | Submitted works | |
|---|---|---|
| nith on 2024-05-30 | | <1% |

| 106 | Internet | |
|---|---|---|
| oa.upm.es | | <1% |

| 107 | Internet | |
|---|---|---|
| studentsrepo.um.edu.my | | <1% |

# INVESTIGATION AND CONTROL ASPECTS OF SOME DC-DC CONVERTERS WITH EV INTEGRATION

**Thesis Submitted**

**in Partial Fulfillment of the Requirements for the**

**Degree of**

# MASTERS OF TECHNOLOGY

**in**

**Power Electronics and Systems**

**by**

**Aneeh Verma**

**(2K23/PES/04)**

**Under the Supervision of**

| | |
|---|---|
| Prof. ALKA SINGH | Prof. RACHNA GARG |
| **(Professor, EED, DTU)** | **(H.O.D, EED, DTU)** |



**To the**

**Department of Electrical Engineering**

# DELHI TECHNOLOGICAL UNIVERSITY

**(Formerly Delhi College of Engineering)**

**Shahbad Daulatpur, Main Bawana Road, Delhi-110042, India**

**MAY, 2025**

# ACKNOWLEDGMENTS

I would like to express my heartfelt gratitude to **Prof.** **Rachna Garg** and **Prof.** **Alka Singh** for their invaluable guidance, unwavering support, and expert insights throughout this journey. Their dedication and expertise have been instrumental in shaping this work.

I am deeply indebted to my senior **Mr. Sudhanshu Mittal** for his consistent guidance, advice, and unwavering belief in my abilities. His seniority and wisdom have been a beacon of light, guiding me at every step.

Lastly, my heartfelt thanks to all my friends who have stood by me, offering support, encouragement, and moments of relief during challenging times. Your camaraderie and companionship have made this journey memorable.

Thank you to everyone who played a part, directly or indirectly, in the realization of this endeavour. Your contributions will forever be cherished.

Date: 31/05/2025

Aneeh Verma

M.Tech (Power Electronics & Systems)

Roll.No 2k23/PES/04

ii

# CANDIDATE'S DECLARATION

I, ANEEH VERMA, Roll No. 2K23/PES/04 hereby certify that the work which is being presented in the thesis entitled "**Investigation and Control Aspects of some DC-DC Converters with EV integration**" in partial fulfilment of the requirements for the award of the Degree of Master of technology, submitted in the Department of Electrical Engineering, Delhi Technological University is an authentic record of my own work carried out during the period from June,2023 to May,2025 under the supervision of Prof. Alka Singh and Prof. Rachna Garg.

The matter presented in the thesis has not been submitted by me for the award of any other degree of this or any other Institute.

**(Aneeh Verma)**

This is to certify that the student has incorporated all the corrections suggested by the examiners in the thesis and the statement made by the candidate is correct to the best of my knowledge.

**Prof. Alka Singh**

**(SUPERVISOR)**

**Prof. Rachna Garg**

**(CO-SUPERVISOR)**

## CERTIFICATE BY THE SUPERVISOR(s)

Certified that **Aneeh Verma** (2k3pes04) has carried out their search work presented in this thesis entitled "**Investigation and Control Aspects of some DC-DC Converters with EV integration**" for the award of **Master of Technology** from thr Department of Electrical Engineering, Delhi Technological University, Delhi, under our supervision. The thesis embodies results of original work, and studies are carried out by the student himself and the contents of the thesis do not form the basis for the award of any other degree to the candidate or to anybody else from this or any other University/Institution.

**Prof. Alka Singh**                                      **Prof. Rachna Garg**

**(SUPERVISOR)**                                      **(CO-SUPERVISOR)**

Place: New Delhi

Date: 31/05/2025

iv

# ABSTRACT

As more and more people around the world use electric cars (EVs) as a more environmentally friendly way to get around, it becomes harder to keep the power grid stable. As more people start using electric vehicles (EVs), large-scale integration might cause problems with voltage drops, phase imbalances, and overloading in the grid infrastructure. In addition, changes in grid voltage and current might make EV charging operations less efficient and less reliable. This thesis suggests an intelligent bidirectional EV charging system that will help solve these problems while making sure that energy flows smoothly between the grid and EV batteries. The suggested system has two main converters: one that converts AC to DC on the grid side and one that converts DC to AC on the EV battery side. A second-order generalized integrator (SOGI)-based technique controls the AC-DC converter. This separates the basic current components from the harmonic distortions, making sure that the power flows in a sinusoidal way. The DC-DC converter uses a constant current charging algorithm to effectively control the battery's voltage and current while it is charging and discharging. These converters work together to create a strong way to transfer energy. They can switch between grid-to-vehicle (G2V) and vehicle-to-grid (V2G) modes while keeping the system stable even when the grid circumstances change.

A lot of simulations with different situations, such as harmonics injection, load changes, and short-term disruptions, to see how well the system works. The results show that the SOGI-based control works well to stop distortions caused by the grid from spreading into charging and discharging currents. The technology also does a great job of regulating voltage, keeping the DC link constant even when the grid supply changes. The bidirectional DC-DC converter smoothly switches between buck and boost modes, making sure that power flows in both ways without harming the battery. The results of this study show that an enhanced EV charging architecture is possible and will improve the stability of the grid while also improving the performance of EV batteries.

# TABLE OF CONTENTS

# List of Tables

ix

# List of Figures

x

xi

# List of Abbreviations

| S.No | Abbreviations | Meaning |
|------|---------------|---------|
| 1. | IC | Internal combustion |
| 2. | EV | Electric Vehicle |
| 3. | OBC | On Board Charger |
| 4. | V1G | Unidirectional Smart Charging |
| 5. | V2G | Vehicle to Grid Charging |
| 6. | V2H | Vehicle-to-Home |
| 7. | SOGI | Second Order Generalized Integrator |
| 8. | PI | Proportional Integrator |
| 9. | PHEV | Plug-in Hybrid Electric Vehicles |
| 10. | BEV | Battery Electric Vehicles |
| 11. | EMI | electromagnetic interference |
| 12. | PV | photovoltaic |
| 13. | WECS | wind energy conversion system |
| 14. | SRM | Switched Reluctance Motor |
| 15. | BESS | Battery Energy Storage System |
| 16. | IPT | Inductive Power Transfer |
| 17. | THD | Total Harmonic Distortion |
| 18. | VSC | voltage source converter |
| 19. | JLHCAF | joint logarithmic hyperbolic cosine robust sparse adaptive filter |
| 20. | PEC | Power Electronic Converter |
| 21. | PWM | Pulse Width Modulated |
| 22. | BSC | Battery Side Converter |
| 23. | GSC | Grid Side Converter |
| 24. | ST | Sine template |
| 25. | UT | Unit template |

xii

# List of Symbols

| S.No | Symbol | Meaning |
|------|--------|---------|
| 1. | $V_1$ | Primary Side Voltage |
| 2. | $V_2$ | Secondary Side Volatage |
| 3. | $S_i$ | $i^{th}$ Switch |
| 4. | $i_{L1}$, $i_{L2}$ | Current through inductor $L_1$ and $L_2$. |
| 5. | $v_{c1}$, $v_{c2}$ | Voltage across $C_1$ and $C_2$ |
| 6. | $D$ | Duty Ratio |
| 7. | $V_{DC}$ | DC Link Voltage |
| 8. | $I_{bat}$ | Battery current |
| 9. | $f_{sw}$ | Switching frequency |
| 10. | $V_{bat}$ | Battery Voltage |
| 11. | $\Delta I_{L1}$ | Current ripple in Inductor $L_1$ |
| 12. | $\Delta I_{L2}$ | Current ripple in Inductor $L_2$ |
| 13. | $\Delta V_{bat}$ | Ripple in battery voltage |
| 14. | $T$ | Time period |
| 15. | $R_L$ | Load resistance |
| 16. | $X_L$ | Load impedance |
| 17. | $I_{bref}$ | Battery reference current |
| 18. | $I_{bm}$ | Measured battery current |

# CHAPTER 1

## Introduction

## 1.1 Background and Motivation

Transportation is an important aspect and convenience for everyone. Traditional vehicles using internal combustion (IC) engines powered with fossil fuels possess a few major drawbacks such as (i) limited power resource as fossil fuel is non-renewable and hence is limited in nature (ii) environmental pollution caused by the burning of fossil fuel. These limitations are mitigated to some extent by the use of EV's [1]. EV's are powered from battery thus causing no pollution. In an attempt to reach the EV 30@30 agreement, India intends to raise the proportion of electric cars (EVs) to 30% of all vehicles sold by 2030 [2]. In India, it is anticipated that 15% of four-wheelers and over 50% of two- and three-wheelers will be electric by 2040 [3].

The rise of electric vehicles (EVs) as a sustainable alternative to conventional internal combustion engine vehicles has led to significant research in power electronics, particularly in the field of battery charging technologies. An onboard charger (OBC) acts as a critical interface between the electrical grid and the EV battery, ensuring efficient and controlled energy transfer. The primary objective of an onboard charger is to provide safe, reliable, and adaptive charging while optimizing energy efficiency.

With the increased integration of EV's into the grid, the power infrastructure may encounter new difficulties such as voltage sags, overloading in grid infrastructure, phase imbalance etc [4]. These problems are mitigated to some extent by incorporating unidirectional controlled charging (V1G) and Vehicle to Grid V2G charging [5]. Frequent charging and discharging have a negative impact on EV-battery, as it causes battery degradation [6]. Further, issues such as grid reliability, voltage and frequency control need to be studied in detail [7]. In order to obtain bidirectional power flow, the chargers need to be designed carefully. Different topologies and different types of chargers for bidirectional charging scheme are discussed in [8].

1

## 1.2 Overview of the System

The proposed onboard charger consists of the following major components:

### 1.2.1 Grid Connection

The electric vehicle's battery and load are both supplied with power by the system, which is directly connected to the grid. The charger was developed to operate under both ideal and distorted grid conditions, with the purpose of evaluating the variations in performance that are caused by harmonic disturbances.

### 1.2.2 Conversion Stage for AC-DC Current in Both Directions

When it comes to rectification and inversion, as well as voltage regulation, a bidirectional AC-DC converter is extremely helpful. A Second-Order Generalized Integrator (SOGI) controller is used to control the switching signals for this converter. This controller is responsible for extracting the fundamental current component from the grid voltage. The performance of the rectifier stage is improved as a result of this approach, which guarantees the reduction of harmonics.

### 1.2.3 DC-DC Conversion Stage

DC-DC converters are responsible for managing the transfer of energy between the AC-DC stage and the electric vehicle battery. These converters have the ability to function in both directions, allowing power to flow both to and from the battery. We investigate two different topologies. It is possible to perform step-up and step-down operations with the help of the Bidirectional Buck-Boost Converter, which enables flexible voltage conversion. The Bidirectional cuk Converter offers a number of additional benefits, including enhanced current ripple management and enhanced voltage regulation. When it comes to regulating the switching of the DC-DC converter, a Proportional-Integral (PI) controller is utilized. This controller ensures that the voltage and current during operation are both stable.

# Chatpter 2

# Literature Review

In this chapter extensive literature review is done.

Paper [9] examines the topology, features, components, operation, strengths, and weaknesses of the various converters used in electric vehicles. The many kinds of electric automobile converter controllers and different techniques of modulation are also examined in this research with regard to their functionalities, advantages, and disadvantages. The important issues and difficulties surrounding converters, controllers, and optimizations for electric automobiles are examined in this study.

Paper [10] examines the development and assessment of various DC-DC converter topologies for Plug-in Hybrid Electric Cars (PHEVs) and Battery Electric Vehicles (BEVs). These converter topologies, design and assessment are illustrated, examined, and discussed in terms of output power, number of components, switching frequency, losses, electromagnetic interference, efficacy, dependability, and cost. The architecture, benefits, and drawbacks of several converter topologies (AC-DC & DC-AC) for fast charging stations (FCHARs) are assessed in this research.

This research [11] investigates a novel wide-range bidirectional dc–dc converter with enhanced voltage gains of the transfer ratio for electric vehicle applications.

Since its initial proposal by Dr. Slobodan Ćuk in 1976, the Cuk converter has attracted a lot of attention because of its unique features, which include continuous input and output currents, reduced electromagnetic interference (EMI), and high efficiency. [12]

Because of its many advantages, the Cuk converter is frequently chosen over other DC-DC converters. One of the main benefits is that the input and output currents are continuous, which reduces ripple currents on both ends and, as a result, harmonics on both the input and output sides. Its consistent input current reduces the input filter capacitor's stress and hence the size that is needed. Furthermore, because the Cuk converter grounds the electronic switch's control terminal, the gate drive design is made simpler overall. [13]-[14]

Paper [15] explains how to build and operate a bidirectional battery charger for electric cars that can also be used as an active power filter by connecting it to the home electrical grid in the area. Additionally, the charger is built and programmed to function both while the battery is being charged from the grid and when power is being returned to it when required.

3

A control of solar photovoltaic (PV) array and wind energy conversion system (WECS) based charging station is presented in this article [16]. The charging station is based on an adaptive frequency-fixed second-order generalized integrator with dc offset rejection capability (AFF-SOGI-DRC). The purpose of this article is to improve the power quality of the grid and to charge electric vehicles (EVs). The purpose of this paper is to discuss a photovoltaic array and a WECS-based multipurpose charging station that incorporates AFF-SOGI-DRC in order to improve power quality at the grid.

The purpose of this study [17] is to design a switched-reluctance motor (SRM) drive for electric vehicles that is driven by a battery/supercapacitor and has grid-to-vehicle (G2V) and vehicle-to-home (V2H)/vehicle-to-grid (V2G) functionalities. Within the scope of this work, the creation of an electric vehicle SRM drive that incorporates battery/SC hybrid storage and boasts G2V, V2H, and V2G features has been demonstrated. An SRM, an asymmetric bridge converter, and a bidirectional front-end dc/dc converter are the primary components that make up the configuration of the system.

DISOC, which stands for non-isolated dual-input single-output dc–dc converter, is a unique converter that is proposed in this [18] study. In accordance with the current state of power availability with PV and battery, as well as the current state of operation of the electric vehicle, the DISOC structure can be modified to carry out six distinct types of operations. When it comes to the integration of the two input sources, the DISO converter topology is the one that is advocated. This converter is capable of functioning in six distinct modes of operation, and it makes efficient use of the electricity generated by photovoltaic solar panels as well as the power that is stored in the battery. Additionally, it is capable of doing V2V or V2G operation when the car is in parking mode, and it does so without the need for any external dc–dc converter whatsoever.

A full analysis is done in [19] on whether it is possible to add EVs to the current distribution system, looking at both slow and fast charging options. The study indicated that the charging station could handle more EVs without overloading the distribution transformer if it could work in both directions (G2V and V2G services).

The research [20] suggests an adaptive error convergence method to make the charging dynamics of an electric vehicle (EV) charging system better in a grid-connected proton-exchange membrane fuel cell (PEMFC) architecture. This paper analytically describes a strong adaptive control that converges more quickly when the grid isn't working properly. This shows how to charge many EVs at once. To stop big voltage swings and electromagnetic instability during multi-source integration, a strong DC link voltage regulation is shown at different control goals. The new PMAE method

4

creates a projection-based change that always affects the gradient of parameter adaptation to keep the control parameters inside a set parameter boundary. This builds a steady DC link for charging in both directions with several goals.

The article [21] suggests an integrated converter (IC) for electric vehicles (EVs) that can charge them via driving, grid-to-vehicle (G2V), vehicle-to-grid (V2G), and DC/vehicle-to-vehicle (V2V) methods. The EVs would use a switching reluctance motor (SRM) for their drive-train. The proposed IC doesn't need any extra non-integrated power electronics parts or inductors to work. In G2V/V2G mode, the winding nodes are directly connected to the AC gird terminals. Also, the new bidirectional G2V/V2G charger lets BESS charge and discharge across an AC grid with any voltage rating. The suggested IC's DC-link can be connected to a DC source or load of any voltage rating for DC/V2V charging because the integrated DC charger can work in all four quadrants.

This [22] study suggests a new, inductively coupled, bidirectional grid interface that doesn't need a dc-link capacitor or an input inductor. It is made up of two converters that are connected back-to-back. For V2G and G2V systems, a bidirectional, contactless grid interface that doesn't need a dc-link capacitor or an input inductor has been suggested. It is based on inductive power transfer (IPT). The proposed grid interface features two converters that are connected back-to-back and can control the flow of electricity in both directions and at different levels. The grid converter can work at a significantly lower switching frequency and with a simpler switching approach than other systems.

The research [23] proposes three novel operational modes for an electric vehicle (EV). (a) home-to-vehicle (H2V) (b) vehicle-for-grid (V4G) (c)Vehicle-to-Home (V2H). In H2V operation mode, the current in the electric vehicle is regulated based on the electrical consumption of household appliances to avert overloads and overcurrent trips in the main circuit breaker. This operational mode occurs during the charging or discharging of the EV battery. In the V4G operational mode, the electric vehicle battery charger is utilized for the compensation of reactive power or current harmonics within the residence. This operational mode can also be executed during the charging or discharging of the EV battery. In the V2H operational mode, the electric vehicle functions as a power source for an isolated residence or as an offline uninterruptible power supply for a grid-connected home. A variety of experimental results are provided, both in steady state and during transients, to validate the previously indicated operational modes and to demonstrate that the electric vehicle can serve as an asset for smart grids and smart households.

This article [24] looks into how bidirectional EVs affect the electrical grid's voltage profile, frequency stability, and power quality. A strategy for optimal frequency

support is suggested that can bring the grid's frequency back to normal in case of problems by using the available EVs inV2G mode. The study found that using EVs during periods when there are more of them at charging stations, particularly at night, can raise the frequency by as much as 0.28 Hz in a low-inertia system and 0.12 Hz in a high-inertial power system. In terms of power quality, light load EVs add more THD to the grid than heavy load EVs with the same total power, up to 35 times more. Also, electric vehicles (EVs) connected to the high-line grid made the grid current have more THD. In several scenarios that were looked at, the THD of EV sets connected to the 240 V grid is almost twice that of the 120 V grid.

The study [25] suggests a way to control active power decoupling for a three-port conversion system with only one phase. Researchers have looked into how to automate the SRCC method for lowering the DC-link capacitance. A Li-ion battery pack was chosen as the best ripple power decoupling part to take the place of the electrolytic capacitor tanks in the PV/battery combination. Even with a tiny dc-link capacitance, the THD of the AC grid current dropped by more than 2%. This study shows that more than 90% of capacitance can be avoided compared to the usual way of power decoupling with DC charging. This means that costs and sizes can be greatly decreased, which means that a very high-power density is possible.

The paper [26] talks about a photovoltaic (PV)-based off-board charging system that is connected to the grid through a voltage source converter (VSC). The joint logarithmic hyperbolic cosine robust sparse adaptive filter (JLHCAF) method is what controls the grid-tied off-board charger. This method does a good job of tracking the main part of the load current over a short period of time, which gives it a good dynamic response.

This paper also talks about a PV-based off-board charger that can work in several ways, such as G2V, V2G, V2H, G2H, and PV2G. The JLHCAF-based control algorithm works better than the LMS control algorithm that is already in use. The JLHCAF algorithm responds quickly to changing conditions when the load changes.

The study [27] looks into, shows, and designs five non-isolated bi-directional dc-dc converter topologies for use in renewable energy producing plants. The non-isolated bi-directional SEPIC dc-dc converter (NBSC) works better than the non-isolated bi-directional CUK dc-dc converter (NBCC) because it has less ripple voltage and a higher output voltage. The input and output current are steady, and there is less ripple in the output current (0.161% of the average output current) and output voltage (1.325% of the output voltage) than in non-isolated bi-directional dc-dc cuk converters. The value of the coupling capacitor doesn't depend on the ripple in the output voltage. Because it changes how it works inside and connects the input and output ports. The value of the internal capacitor (also called the coupling capacitor) is 20 times lower than the value of the output capacitor.

6

The paper [28] talks about how to develop a good control strategy for a non-isolated bidirectional DC-DC converter. The converter in question has a basic design and a high voltage gain. The proposed converter has a higher voltage gain in step-up mode than a standard converter. The converter contains four power switches, but only two of them can be used at a time. Two inductors on the input side split the input current, which lets you use smaller inductors. The proposed converter is easy to build and works well.

The paper [29] looks at the most advanced EV charging topologies and PEC solutions for EV applications in great detail. It looks into PECs in terms of their types, setups, ways of controlling them, and future research opportunities, as well as how they affect power quality. This study looks at the charging topologies of electric vehicles (EVs) in terms of where they are located, how much power they can handle, how they connect physically, and the direction of the power flow. In addition, a thorough study of PEC solutions for EV applications has been done, looking at their circuit layouts, switching patterns, structure, and control methods based on recent article reviews. We also looked into the different PEC topologies that use DC-DC converters, AC-DC converters, DC-AC converters, and AC-AC converters for building, types, modulation techniques, and control schemes for high-voltage and low-voltage applications, mostly for EV charging stations. Along with showing the soft switching converters, the multilayer converters, and the multiport converters, these are also contemporary solutions for power train problems in electric vehicle applications. Next, we'll look at the main forecasts, problems, and effects of the PECs on the vehicle system and the power quality of the utility grids based on current review articles.

The article [30] looks at the most advanced designs for off-grid and hybrid charging systems and looks into their different subsystems, like power electronics converters, energy storage systems, single or multiple energy sources, and energy management algorithms. This article has looked into and talked about the many designs of off-grid and hybrid charging systems for electric vehicles. It also looked at and studied their different subsystems, like energy sources, ESS, PECs, EMS, and charging connectors (their power level and standards) for different sorts of vehicles.

The paper [31] looks at the most important topologies that have been used in recent research to create fully integrated slow (single-phase) and fast (three-phase) on-board EV battery charging systems using either induction or permanent magnet motors. It focuses on topologies that don't require much or any hardware reconfiguration. This research looked at the best integrated onboard chargers available for electric vehicles. We talked about several kinds of chargers and looked at their pros and cons. There have also been talks on different kinds of converters, drivetrains used in EVs, charging control methods, and technical problems. Also, it was shown how to use either three-

7

phase or multiphase machines for sluggish (single phase) and quick (three phase) charging.

The article [32] gives a full overview of EV charging technologies, worldwide standards, the design of EV charging stations, and the different ways that EV charging systems can convert power. This article has looked at the different types of EV charging technologies, standards, charging station layouts, and power converter combinations. We look at several sorts of electric vehicles (EVs), charging levels, modes, connectors, and batteries to see how charging technologies and needs are doing. A comparison of the charging station architecture has been made based on AC/DC power flow, control approach, pros and cons. Most multiport EV charging stations include solar panels and batteries built in to help the power grid and offer other services.

The paper [33] talks about the most advanced topologies and control approaches for off-board chargers' ac-dc and dc-dc power stages. It focuses on technical specifics, ongoing progress, and problems. Also, most of the newer multiport EV chargers that combine PV, energy storage, EV, and the grid are shown. This document goes into great length about the current state, technical specifics, and problems with the power converter topologies and their control mechanisms for EV off-board chargers. A study that compared different power converter topologies based on factors like power, frequency, voltage range, THD, peak efficiency, and switching modulation, as well as their pros and cons, has been done. This article talks about the three-port and four-port converters that are currently used to charge electric vehicles. Close attention is kept at the control mechanisms for ac-dc rectifiers and dc-dc converters that are used for fast charging EVs.

The paper [34] presents a non-isolated onboard charger (OBC) utilizing an interleaved bidirectional buck/boost converter. The OBC is designed for 1kW operation. The performance of the OBC during the G2V operation amidst grid voltage fluctuations is validated. The charging process with a 15A current has been validated via simulation. This operation is validated through hardware experimentation. The performance of the OBC during V2G operation is examined.

The article [35] examines the design and regulation of a bidirectional battery charger for electric vehicles, as well as its function as an active power filter when integrated with the local residential electrical grid. The charger is engineered and regulated to function while charging the battery from the grid and to inject electricity back into the grid as necessary. This work presents the design, analysis, and simulation of a bidirectional electric vehicle charger comprising a voltage source inverter (VSI) AC/DC converter and a dual active bridge (DAB) DC/DC converter. This charger is

8

designed for battery charging (G2V operation), battery discharging to the grid (V2G operation), and active filtering when connected to the home.

Since its initial proposal by Dr. Slobodan Ćuk in 1976, the Cuk converter has attracted a lot of attention because of its unique features, which include continuous input and output currents, reduced electromagnetic interference (EMI), and high efficiency [36]. Because of many advantages [36], the Cuk converter is frequently chosen over other DC-DC converters. One of the main benefits is that the input and output currents are continuous, which reduces ripple currents on both ends and, as a result, harmonics on both the input and output sides. Its consistent input current reduces the input filter capacitor's stress and hence the size that is needed. Furthermore, because the Cuk converter grounds the electronic switch's control terminal, the gate drive design is made simpler overall. [37-38].

Authors in [39] discuss SOGI controller in detail. SOGI block is used to attenuate the high frequency terms in the ac -dc converter. An on-board bidirectional EV charger is proposed in this paper which rejects the harmonics effects of the grid. The SOGI controller is used to generate the gate pulses for the switches of ac-dc converter. Pulse width modulation (PWM) control scheme is used to control the bidirectional dc-dc converter at the EV side. The simulation results are discussed in detail under various grid scenarios for both the charging/ discharging modes of operation.

This work [40] discusses the design, modeling, and simulation of an analog-controlled bi-directional buck-boost converter. The model emphasizes the significance of non-linear characteristics in voltage converters, including the equivalent series resistance (ESL) of the inductor, the equivalent series resistance (ESR) of the capacitor, and the on-resistance (RDS(on)) of MOSFET switches. Analog controllers are constructed with type I, II, or III compensation. Simulations of a bi-directional buck-boost converter are conducted using Matlab/Simulink. The operation of the converter using an analog controller has also been demonstrated.

Calculation of different elements of the dc-dc buck converter has been described in the paper [41]. Authors of the paper [42] have described the calculation for the elements present in the dc-dc boost converter.

This work [43] presents a comprehensive mathematical model of a DC-DC Cuk converter functioning in continuous conduction mode. Averaged large signal model is initially derived via the State-Space averaging method. The steady-state model and small-signal model are derived through linearization, enabling the determination of different transfer functions of the Cuk converter for control design purposes. The model validation is conducted by simulating a physical model of the Cuk converter using the PSIM simulator and then comparing the results with the outcome of the mathematical simulation derived from MATLAB Simulink. The authors in [44]

9

describe the designing of the controller for the cuk converter using model order reduction.

10

# Chapter 3

## Design and Modelling Of Different DC-DC Converter

In this chapter design and modelling of two non-isolated bidirectional converter is discussed.

## 3.1 Bidirectional buck and boost converter.

The figure for this converter is shown in Fig.3.1. This converter operates in either buck or boost mode. Operating mode is selected by the PWM signal to the switches. This converter consists of two switches. Each switch consists of a Mosfet and anti-parallel diode for the bidirectional power flow.

In either of the two modes of operation (buck or boost mode), one of the switch turns on and off and the corresponding anti-parallel diode remains off for the whole operation whereas, the diode of the other switch acts as passive (naturally commutated) switch.

For modelling, both the modes are studied separately and then merged to get the operating parameters values [40].
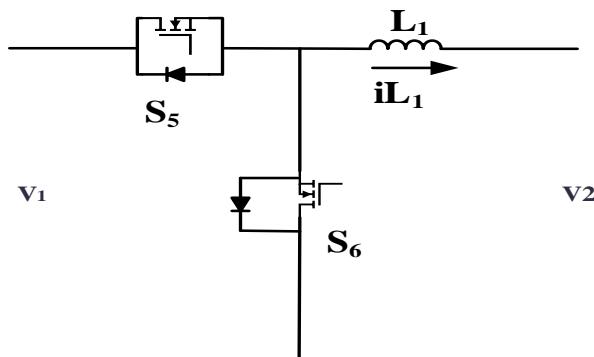


Fig.3.1.  Bidirectional buck and boost converter

### 3.1.1 Buck Operation Mode

In the buck mode, the power is transferred from primary side ($V_1$) to secondary side ($V_2$). Fig. 3.2.(a) represents the working of normal buck converter and Fig. 3.2.(b) represents the equivalent circuit of proposed EV- battery side converter in the buck mode (the complete system model will be discussed in further chapters). The design of L and C values is discussed below.

11
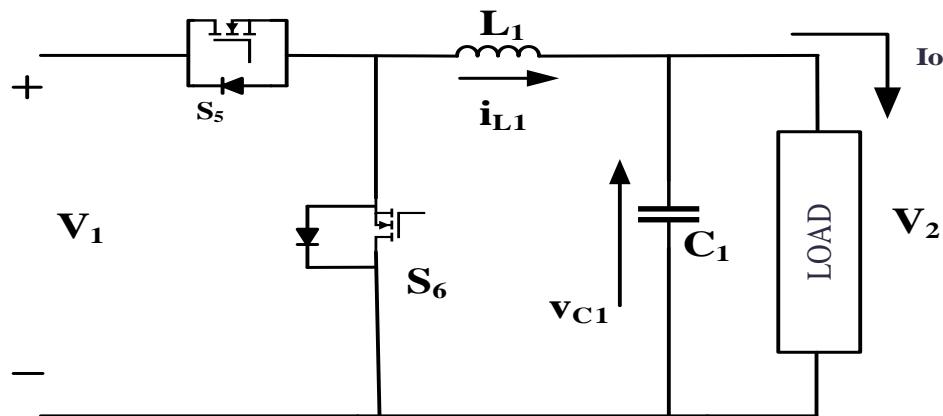
Fig. 3.2.(a). Buck mode of buck & boost converter

### A. Inductor Design

As given in the [41] the inductor $L_1$ is designed using equation (3.1).

$$L_1 = \frac{(1-D)*V_2}{\Delta I_L * f_{sw}} \tag{3.1}$$

where, D = duty ratio and is equal to $V_2 / V_1$.

$\Delta I_L$ = ripple in inductor current

$V_2$ = secondary side voltage

$f_{sw}$ = switching frequency

Now above equation with respect to Fig. 3.2(b) can be given as

$$L_1 = \frac{(1-D)*V_{bat}}{\Delta I_L * f_{sw}} \tag{3.2}$$

$$D = \frac{V_{bat}}{V_{DC}} = \frac{260}{400} = 0.65 \tag{3.3}$$

$$L_1 = \frac{(1-0.65)*260}{0.05*20*10000} = 9.1 mH \tag{3.4}$$

In equation (3.2) $V_2$ from equation (3.1) is replaced by $V_{bat}$. Inserting values of the variables from the Table I, $L_1$ is obtained. The value of $L_1 = 9.1$ mH. Ideally the final selected value is taken as 1.25 of the calculated value i.e $L_1 = 1.25*L_1$. Thus, the designed value of $L_1$ for buck operation is given by $L_1 = 12$ mH.

### B. Capacitor Design

The value of filter capacitor for buck converter is obtained from [41] and represented as the given equation

12

$$C_1 = \frac{V_2*(1-D)}{8*L_1*f_{sw}^2*\Delta V_2} \qquad (3.5)$$

With respect to the proposed model as in Fig 3.2(b) equation (3.5) is rewritten as

$$C_1 = \frac{V_{bat}*(1-D)}{8*L_1*f_{sw}^2*\Delta V_{bat}} \qquad (3.6)$$

$$C_1 = \frac{280*(1-0.65)}{8*12*10^{-3}*10000^2*0.05*280} = 0.729\mu F \qquad (3.7)$$

inserting values of the variables from the Table 1, we get $C_1$ as $C_1 = 0.729\mu F$. For practical consideration $C_1$ as approximated as 10µF.
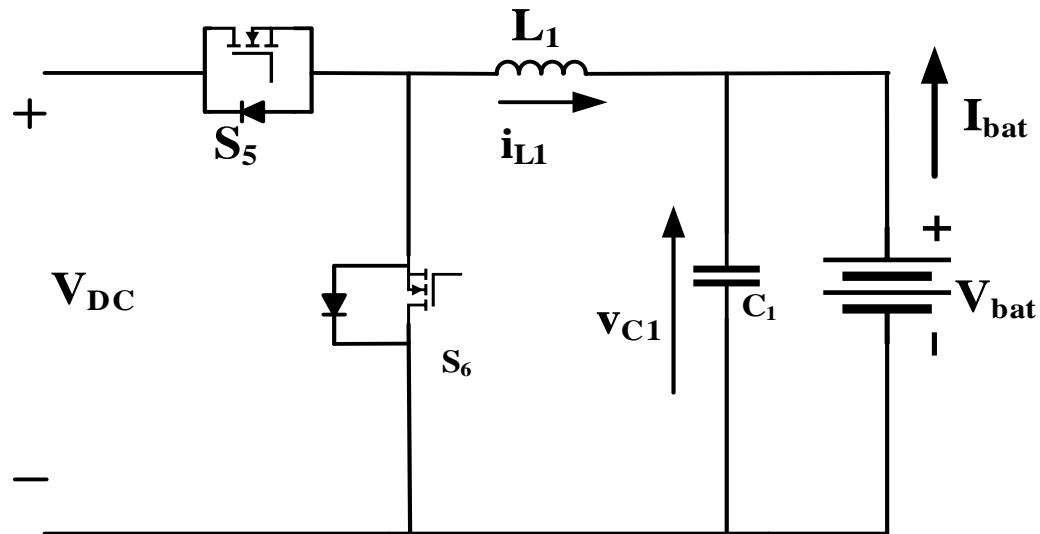


Fig. 3.2.(b). Proposed model equivalent in buck mode.

13

### 3.1.2 Boost operation mode

In the boost mode the power is transferred from secondary side ($V_2$) to primary side ($V_1$). Fig.3.3.(a) represents the working of normal buck converter and Fig.3.3.(b) represents the equivalent circuit of proposed EV- battery side converter in the boost mode. Following section discusses the design of inductor (L) value.

As mentioned in [42] the value of inductor is given as:
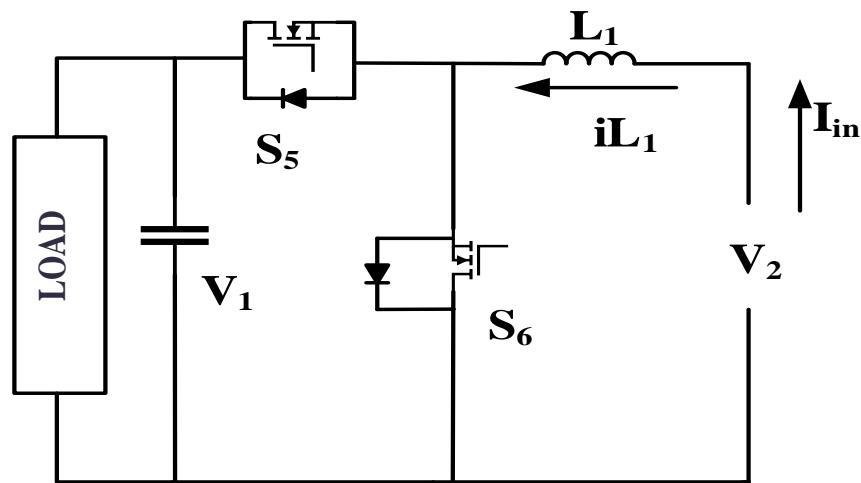


Fig. 3.3.(a). Boost mode of buck & boost converter

$$L_{\min} = \frac{D*(1-D)*V_1}{2*f_{sw}*I_{in}}$$  (3.8)
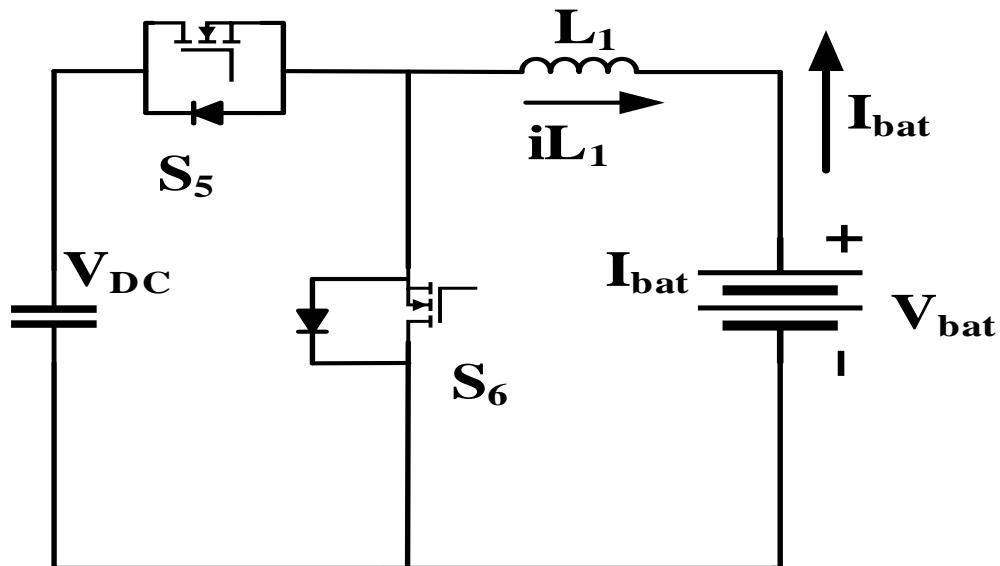


Fig. 3.3.(b). Proposed model equivalent in boost mode

14

where D = duty ratio and is equal to $(V_1 - V_2) / V_1$

$f_{sw}$ = switching frequency

$I_{in}$ = input current

$V_{in}$ = input voltage

Equation (3.8) is rewritten as equation (3.9) by replacing the boost converter with the parameters of the actual proposed converter model as shown in Fig. 3(b)

$$L_{\min} = \frac{D*(1-D)*V_{DC}}{2*f_{sw}*I_{bat}} \tag{3.9}$$

$$\text{Here } D = (V_1 - V_2)/V_1 \tag{3.10}$$

$$D = \frac{V_{DC} - V_{bat}}{V_{DC}} \tag{3.11}$$

$$D = 0.35$$

Applying the values from table I in (3.9) we get

$$L_{min} = \frac{0.35*(1-0.35)*400}{2*10000*20} = 0.2275 \text{ mH} \tag{3.12}$$

Again, considering L as 1.25 times the calculated value we get L = 0.285mH.

Thus, we have two values of the inductor one from the buck mode of operation and the other from the boost mode of operation. The final value of L is the maximum value obtained in both the cases. Thus, the designed value of L is selected as 24mH. The output filter capacitor is C = 10μF.

Table I: Selection of parameters for buck and boost converter.

| S.No | Parameters | Values |
|------|-----------|--------|
| 1. | $V_{dc}$ | 400 V |
| 2. | $V_{bat}$ | 280 V |
| 3. | Inductor $L_1$ | 24mH |
| 4. | Capacitor $C_1$ | 10uF |
| 5. | Charging & discharging current $I_{bat}$ | 20A |
| 6. | Operating Frequency | 10 KHz |
| 7. | $\Delta I_{L1}$ | 5% of $I_{bat}$ |

15

| 8. | $\Delta V_{bat}$ | 5% of $V_{bat}$ |
|---|---|---|

## 3.2 Bidirectional Cuk converter

The **Ćuk converter** is a type of DC-DC power converter designed to efficiently change electrical energy between different voltage levels. Invented by **Slobodan Ćuk**, this converter is notable for its ability to provide a smooth, continuous current at both its input and output terminals, making it a popular choice in applications requiring stable power delivery.

Cuk converter is a $4^{th}$ order, non-isolated, switch-mode power converter. The converter consist of two switches ($S_5$ & $S_6$), two capacitors ($C_1$ & $C_2$) and two inductors ($L_1$ & $L_2$) as shown in Fig 3.4.
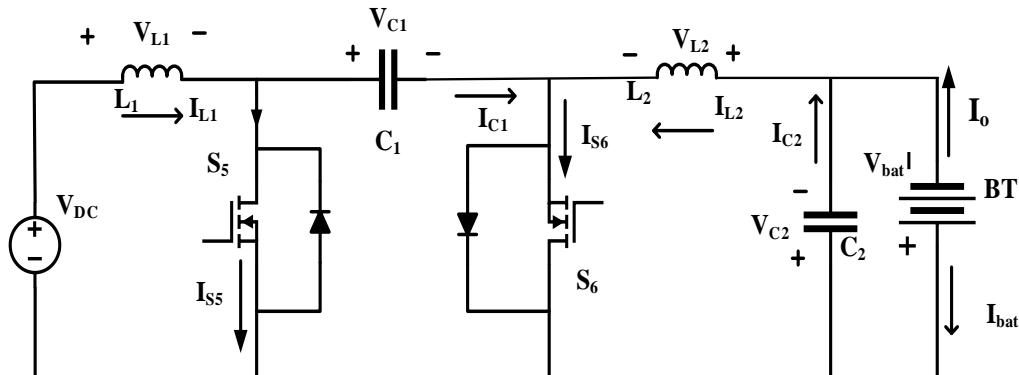


Fig. 3.4. Schematic diagram of the Cuk converter

### 3.2.1 Working of cuk converter

Working of the Cuk converter can be studied under two modes [43]. There are two switches $S_5$ & $S_6$. These switches are also made up of mosfet and an anti-parallel diode. This is done to obtain bidirectional power flow.

16

### A. *Mode A: (S5 is CLOSE and S6 is OPEN)*

In this state switch $S_5$ is CLOSE and switch $S_6$ is OPEN. The resultant circuit is shown in Fig. 3.5.(a).
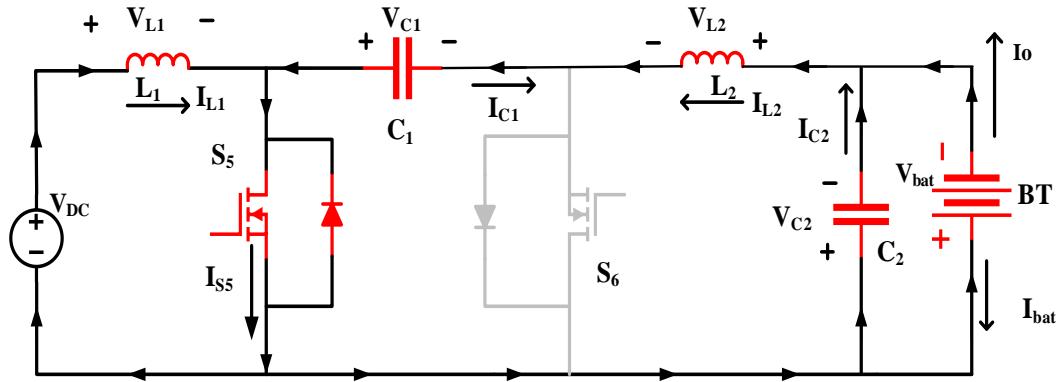


Fig.3.5.(a) Cuk converter in mode A (switch S5: ON and switch S6: OFF)

Applying KVL in the outermost loop gives:

$$V_{C1} = V_{DC} + V_{bat} \tag{3.13}$$

Applying KVL in the DC source loop gives:

$$V_{L1} = V_{DC} \tag{3.14}$$

Applying KVL in the battery side loop gives:

$$V_{L2} = -V_{bat} - V_{C1} \tag{3.15}$$

$$V_{L2} = -V_{bat} + V_{DC} + V_{bat} \tag{3.16}$$

$$V_{L2} = V_{DC} \tag{3.17}$$

### B. *Mode B: (S5 is OFF and S6 is ON)*

In this mode switch $S_5$ is OFF and switch $S_6$ is ON. The resultant circuit is shown in Fig 3.5.(b).

17
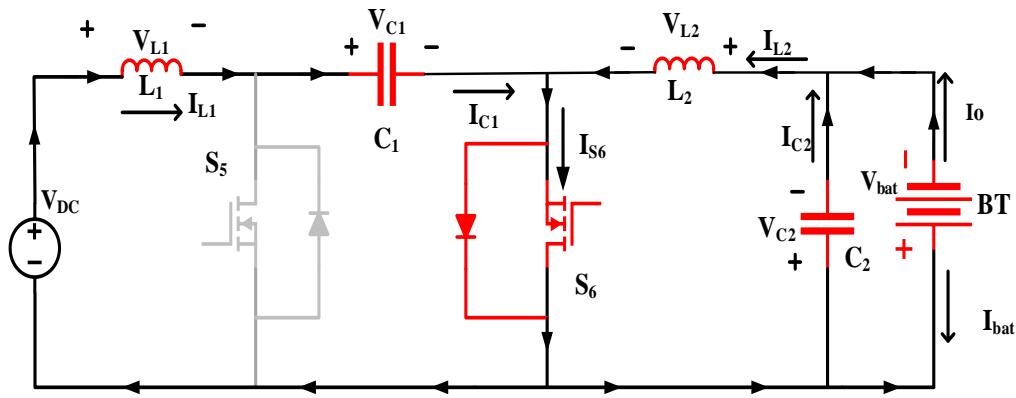
Fig 3.5.(b). Cuk converter in mode B (switch S5: OFF and switch S6: ON)

Applying KVL in the DC source loop gives:

$$V_{L1} = V_{DC} - V_{C1} \tag{3.18}$$

$$V_{L1} = V_{DC} - (V_{DC} + V_{bat}) \tag{3.19}$$

$$V_{L1} = -V_{bat} \tag{3.20}$$

**On averaging:**

Average voltage across an inductor is zero. Therefore,

$$V_{L1} * D + V_{L1} * (1 - D) = 0 \tag{3.21}$$

$$V_{DC} * D - V_{bat} * (1 - D) = 0 \tag{3.22}$$

$$V_{bat} = \frac{V_{DC}*D}{(1-D)} \tag{3.23}$$

$$D = \frac{V_{bat}}{V_{DC} + V_{bat}} \tag{3.24}$$

$$D = \frac{280}{400+280} = 0.411 \tag{3.25}$$

*C.  Determination of converter's passive elements L1, L2, C1 & C2*

These values are based upon the values of current and voltages ripples:

**Calculation of L1:**

In switch S5 is on, from equation 3.14

$$V_{L1} = V_{DC}$$

18

$$L_1 * \frac{dI_{L1}}{dt} = V_{DC} \tag{3.26}$$

$$L_1 * \Delta I_{L1} = V_{DC} * (DT) \tag{3.26}$$

$$L_1 = \frac{V_{DC}*D}{\Delta I_{L1}*f} \tag{3.27}$$

$$L_1 = \frac{400*0.411}{0.05*20*10000} = 16.4\text{mH} \tag{3.28}$$

$$L_1 = 1.25 * 16.4 = 20.5 \; mH \tag{3.29}$$

$$L_1 \cong 20 \; mH \tag{3.30}$$

**Calculation of L₂:**

In switch $S_5$ is in ON condition, from equation 3.17

$$V_{L2} = V_{DC}$$

$$L_2 * \frac{dI_{L2}}{dt} = V_{DC} \tag{3.32}$$

$$L_2 = \frac{V_{DC}*D}{\Delta I_{L2}*f} = L_1 \tag{3.33}$$

$$L_2 \cong 20 \; mH \tag{3.34}$$

**Calculation of C₁:**

In switch $S_6$ is in off condition:

$$I_{C1} = I_{L2} = I_o \tag{3.35}$$

$$I_{C1} = C_1 \frac{dV_{C1}}{dt} = I_0 \tag{3.36}$$

$$C_1 = \frac{I_o*D}{\Delta V_{C1}*f} \tag{3.37}$$

$$C_1 = \frac{20*0.411}{0.05*680*10000} = 24 \; \mu F \tag{3.38}$$

We take C₁ as 1.25*C₁

$$C_1 = 1.25 * 24 \mu F \tag{3.39}$$

$$C_1 = 30 \mu F \tag{3.40}$$

**Calculation of C₂:**

We know that

$$Q = Cdv = \int i_c dt \tag{3.41}$$

$$Q_C = \int_{T/4}^{3T/4} i_{C_2} dt = \frac{1}{2} * \frac{T}{2} * \frac{\Delta I_{L2}}{2} = \frac{\Delta I_{L2}}{8*f} \tag{3.42}$$

19

$$C_2 * \Delta V_{C2} = \frac{\Delta I_{L2}}{8*f} \tag{3.43}$$

$$C_2 = \frac{\Delta I_{L2}}{8*f*\Delta V_{C2}} \tag{3.44}$$

$$C_2 = \frac{0.05*20}{8*10000*0.05*280} = 0.892 \tag{3.45}$$

$$C_2 = 1.25 * C_2 \tag{3.46}$$

$$C_2 \cong 2\mu F \tag{3.47}$$

Where:

 f = switching frequency,

D = duty ratio

T = time period

$V_{DC}$ = source side DC voltage

$V_{bat}$ = voltage across battery

$\Delta V_{C1}$ = voltage ripple in Capacitor $C_1$

$\Delta V_{C2}$ = voltage ripple in Capacitor $C_2$

$\Delta I_{L1}$ = current ripple in Inductor $L_1$

$\Delta I_{L2}$ = current ripple in Inductor $L_2$

Table II consists of values of the all the parameters used in Cuk converter an parameters used to design the Cuk converter.

Table II: Parameters Values for the Cuk Converter

| S.No | Parameters | Values |
|------|------------|--------|
| 1. | Input voltage | 400 V |
| 2. | Output voltage | 280 V |
| 3. | Inductor $L_1$ | 20mH |
| 4. | Inductor $L_2$ | 20mH |
| 5. | Capacitor $C_1$ | 30μF |
| 6. | Capacitor $C_2$ | 2μF |
| 7. | Charging current $I_{bat}$ | 20A |

20

| | | |
|---|---|---|
| 8. | $\Delta I_{L1} = \Delta I_{L2}$ | 5% of $I_{bat}$ |
| 9. | $\Delta V_{C1}$ | 5% of $V_{C1}$ |
| 10. | $\Delta V_{C2}$ | 2% of $V_{C2}$ |
| 11. | Operating Frequency ($f_{sw}$) | 10 KHz |

21

# Chapter 4

# Performance Analysis of Grid Connected EV Charger using Bidirectional Buck and Boost Converter

## 4.1 System Design

The suggested configuration is represented in Fig. 4.1. The system is made up of two bidirectional converters, the first is Grid Side Converter (GSC) and the second is Battery Side Converter (BSC). Both the bidirectional converters interact with each other via a common DC link having DC link voltage of $V_{DC}$.

In G2V mode, the bidirectional AC-DC grid side converter (GSC) feeds energy to the battery through a DC link capacitor by acting as a rectifier. On the other hand, in V2G mode the load is fed by the battery and the remaining energy is fed into the grid. A bidirectional buck and boost converter is used to connect the DC link and the battery of the EV. The bidirectional DC-DC converter can run in either of the two modes i.e., in buck or boost mode. In G2V mode, the DC-DC buck and boost converter is utilized as to charge the battery at constant DC current, here the DC-DC converter works in buck mode. The bidirectional buck and boost converter operates in boost mode in V2G mode, supplying energy to the load and grid.

The battery with bidirectional BSC is connected at DC link of GSC. Further, the interfacing inductor Lc with GSC is connected at common point of the load and the grid. A non-linear active load is considered for simulation purposes.

22
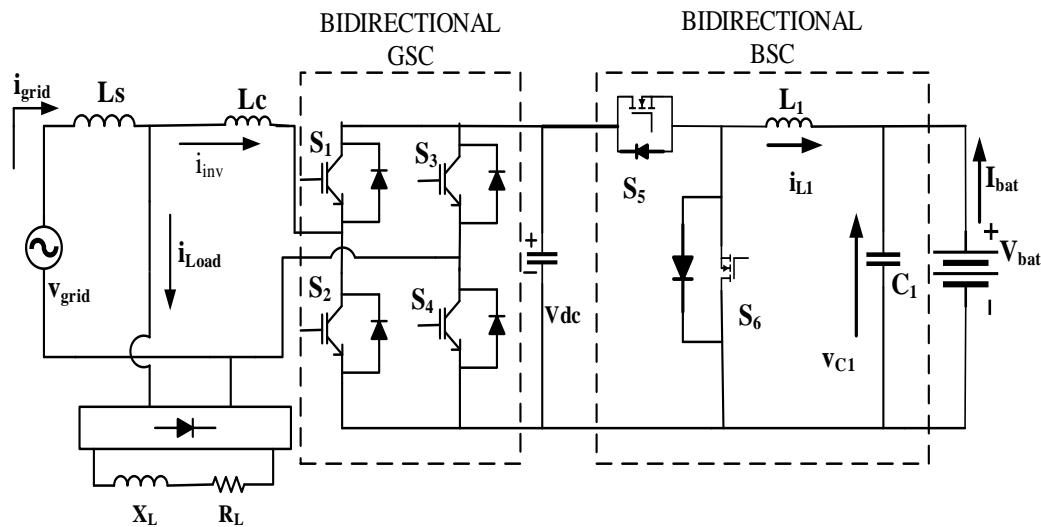
Fig.4.1. Circuit diagram of complete system with bidirectional GSC & bidirectional BSC.

## 4.2 Controller Design:

Design of controller for Battery Side Converter and Grid Side Converter is discussed in this section.

### 4.2.1 Battery side converter

The EV-battery charging/discharging is controlled using constant current mechanism. The direction of current going out of the battery positive terminal is taken as positive.

#### A. Charging Mode

In grid-to-EV-battery (BATTERY CHARGING) mode, the battery keeps charging in this mode the battery's current is negative as the current is entering into the battery via the positive terminal. Thus, a negative reference current (*i.e $I_{bref}$ is negative*) is chosen and compared with the measured battery's current to obtain the error signal which then fed to a PI controller. The output of the PI controller is fed into the PWM generator which finally outputs the gate pulses for the switches $S_5$ and $S_6$. This is shown in the Fig.4.2. Here $I_{bref}$ and $I_{bm}$ denote the reference current in charging or discharging mode and the measured battery current respectively.

#### B. Discharging Mode

In the V2G (BATTERY DISCHARGING) mode that is when EV-battery is supplying the energy to the grid and load, the battery current is positive as the current is leaving the battery from the positive terminal. In this mode a positive reference current (*i.e $I_{bref}$ is positive*) is compared to obtain the error signal which is then fed to the PI controller. Switching signals for the switches of $S_5$ and $S_6$ is obtained in the similar fashion as in the grid-to-EV-battery (CHARGING) mode.

23
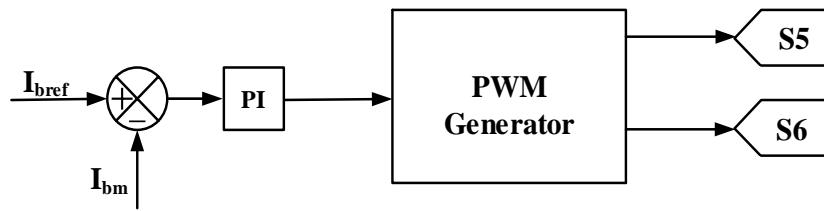
Fig.4.2. Controller for EV-battery side converter

## 4.2.2 Grid Side Converter

The gate pulses for the switches of the grid side bidirectional converter are generated with the help of a SOGI controller and a sine template. The SOGI controller is used to generate the fundamental load current '$I_{fund}$' & sine template is used to generate the reference current used for the switching of bidirectional grid side ac-dc converter.

Fig.4.3 represents the complete control strategy and generation of gating pulses for the Grid side converter.
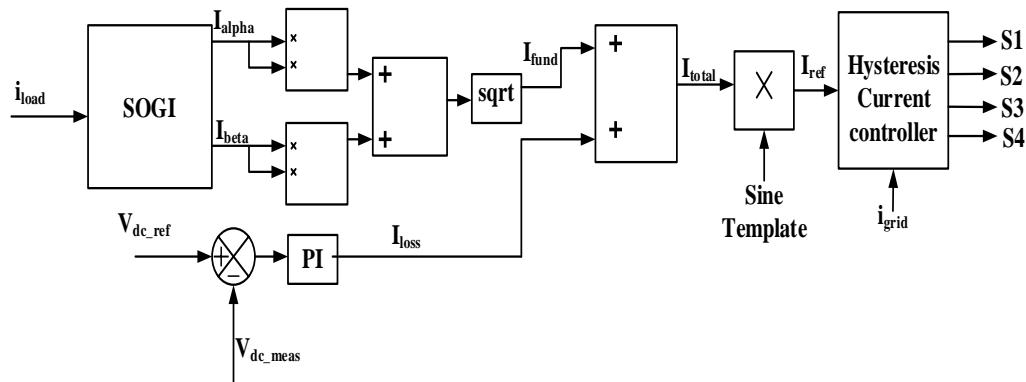


Fig. 4.3. Complete control of grid side converter

The load current is fed into the SOGI controller. $I_{alpha}$ and $I_{beta}$ are the two output of the SOGI controller which are quadrature to each other.

The figure 4.4 represents the working of the SOGI converter. Here $\omega = 2*pi*50$, the fundamental frequency in radians. The working and design of the SOGI converter is studied in paper (39). From the literature, it is significant that the working of SOGI depends on the parameter K, for the optimum operation value of K is selected as K = 0.707 (as conclude from the same paper).

24
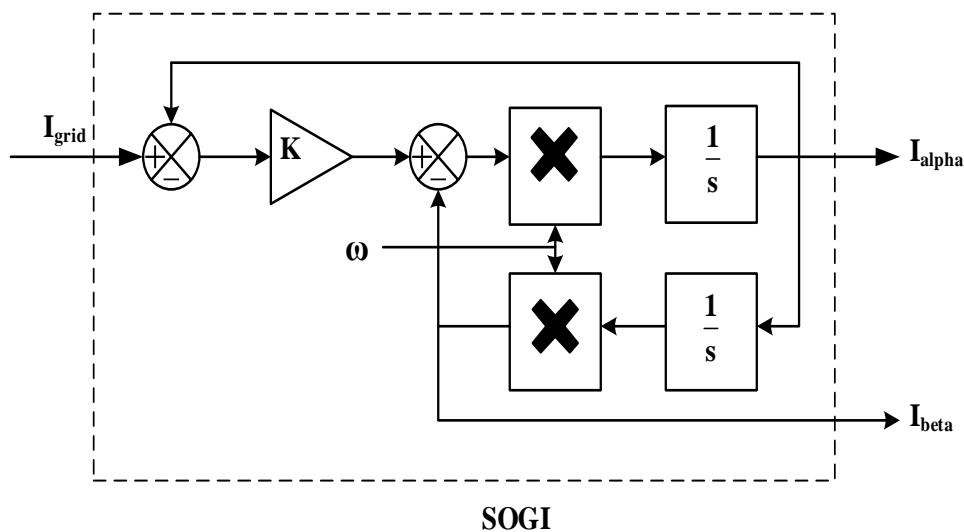
**SOGI**

Fig.4.4. Generation of I $_{alpha}$ and I $_{beta}$ with SOGI controller

$I_{alpha}$ being in phase with the load current. '$I_{fund}$' is the fundamental component of the load current and it is obtained from $I_{alpha}$ and $I_{beta}$ using equation 4.1.

$$I_{fund} = \sqrt{I_{alpha}^2 + I_{beta}^2} \qquad (4.1)$$

In order to calculate the switching losses and maintain desired DC bus voltage, the error between the reference DC bus voltage '$V_{dc\_ref}$' and the measured DC bus voltage '$V_{dc\_meas}$' is fed into a PI controller. The output of the PI controller is '$I_{loss}$'. In order to get the total load current '$I_{total}$' both the signals '$I_{loss}$' and '$I_{fund}$' are added as given by equation 4.2.

$$I_{total} = I_{fund} + I_{loss} \qquad (4.2)$$

In order to obtain reference load current '$I_{ref}$' the total current obtained above is multiplied with a sine template (ST) as given by equation 4.3.

$$I_{ref} = I_{total} * ST \qquad (4.3)$$

The method to obtain the sine template from the grid voltage is explained in the figure 4.5. A delay block (which provides a phase shift of 90 degrees) is used to obtain '$V_{alpha}$' and '$V_{beta}$' from the grid voltage '$V_{grid}$'. The Sine Template (ST) is obtained using equation 4.4.

$$ST = \frac{V_{alpha}}{\sqrt{V_{alpha}^2 + V_{beta}^2}} \qquad (4.4)$$

25
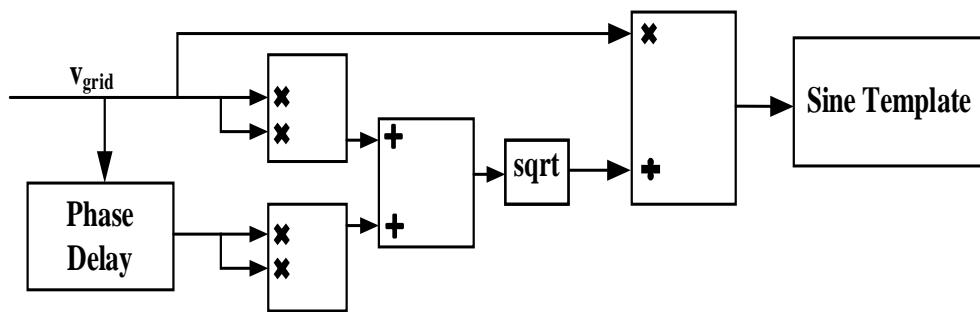
Fig. 4.5. Method to obtain sine template

After getting the reference load current 'I$_{ref}$', both the signals are fed into a hysteresis current controller in order to finally obtain the gating pulses to the four switches S$_1$ S$_2$ S$_3$ and S$_4$ of the bidirectional grid side ac-dc converter as shown in Fig.4.3.

## 4.3 Results Analysis

A Simulink model is developed and working analysis under G2V and V2G is achieved. A detailed discussion is discussed in following sections:

### 4.3.1 Charging and Discharging mode

The Simulink model simulation results for grid voltage, grid current, load current, inverter current, voltage at DC bus, battery voltage, battery current, %SOC (State Of Charge), in Fig.4.6, for both the modes G2V as well as V2G mode. The bidirectional buck and boost converter is designed for DC bus voltage of 400V, battery rating is selected as 280V, 25Ah.

As seen from Fig. 4.6.(a) & 4.6.(b) the grid voltage and grid current are in same phase in charging *i.e.,* G2V mode which states that power is being supplied from grid to the EV-Battery. Also, at some instant (t=0.55s) the model is made to operate in V2G *i.e.,* battery discharging mode. It can be seen from Fig. 4.6.(b) that the grid current is now in phase opposition to grid voltage, which states that battery is supplying current to the grid, hence the energy flow occurs from the EV-Battery to grid. Also, while charging (from time t = 0s to time t = 0.55s) the battery current is negative as observed from

26
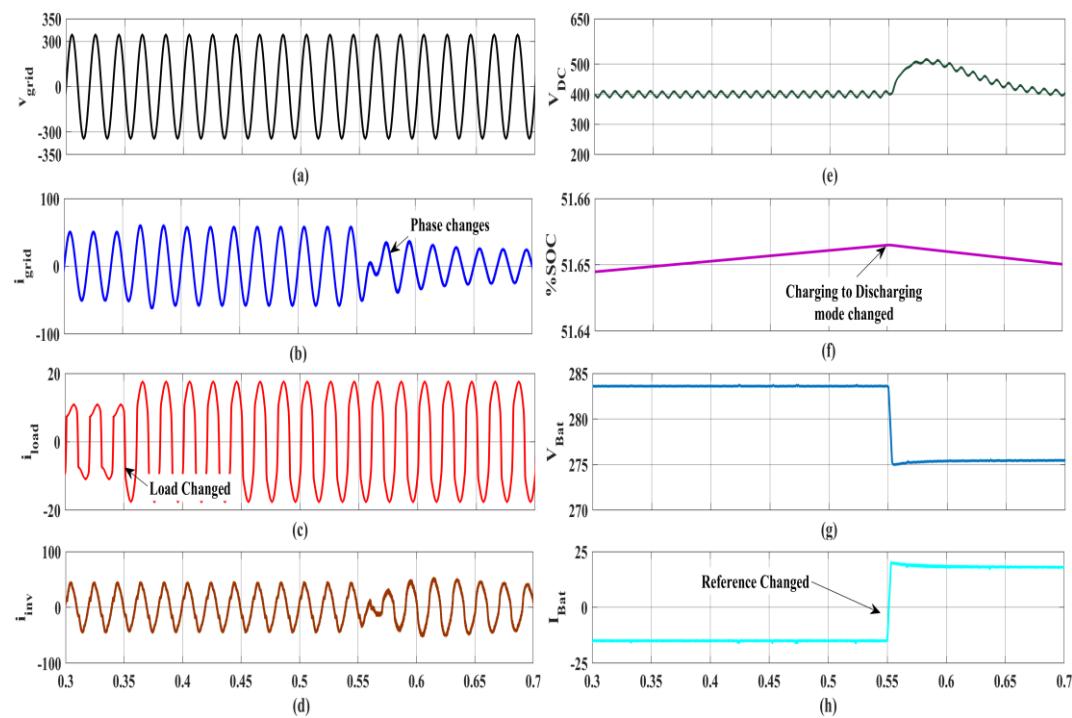
Fig. 4.6. Charging and discharging modes of operation (a) $v_{grid}$ (b) $i_{grid}$ (c) $i_{load}$ (d) $i_{inverter}$ (e) $V_{DC}$ (f) %SOC (g) $V_{Bat}$ (h) $I_{bat}$

Fig.4.6.(h) which is an indicator of battery being charged on the other hand while discharging (from time t = 0.55s to time t = 0.7s) the battery current is positive.

## 4.3.2 G2V with load and current reference variation

The model is designed to charge the battery with up to 20 A current. In the Fig.4.7, the load is changed at t = 0.35s, the Fig.4.7.(h) shows even if there are load changes the designed model can still charge the battery at designed value of current. Increasing the load increases the power demand from the grid as a result more current is drawn, from the grid, also changing the load should not affect the charging current of the battery, both of these statements are verified from the Fig.4.7.(a)-4.7.(d), 4.7.(h). Fig. 4.7.(h) also illustrate that the designed model can also perform well if battery is required to charge at other current level. Here the battery reference is varied from 15A to 18A at t = 0.5s. Increasing the battery charging reference current increases the current drawn from the grid which is also reflected as increased inverter current Fig. 4.7.(d).

27
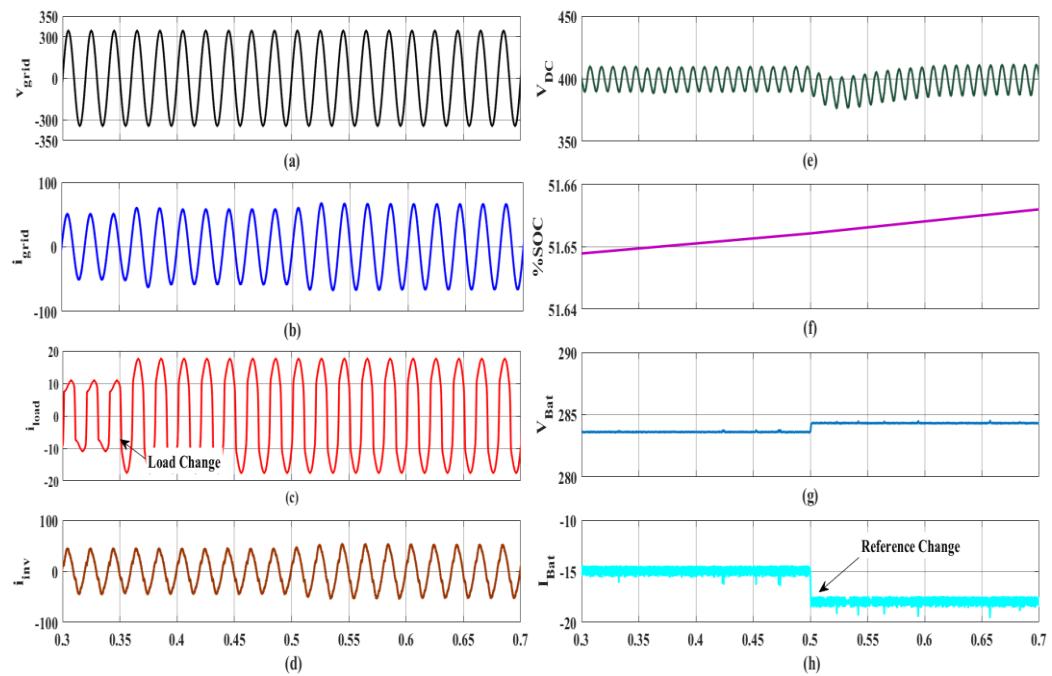
Fig. 4.7. G2V varying load and reference change, (a) v$_{grid}$ (b) i$_{grid}$ (c) i$_{load}$ (d) i$_{inverter}$ (e) V$_{DC}$ (f) %SOC (g) V$_{Bat}$ (h) I$_{bat}$
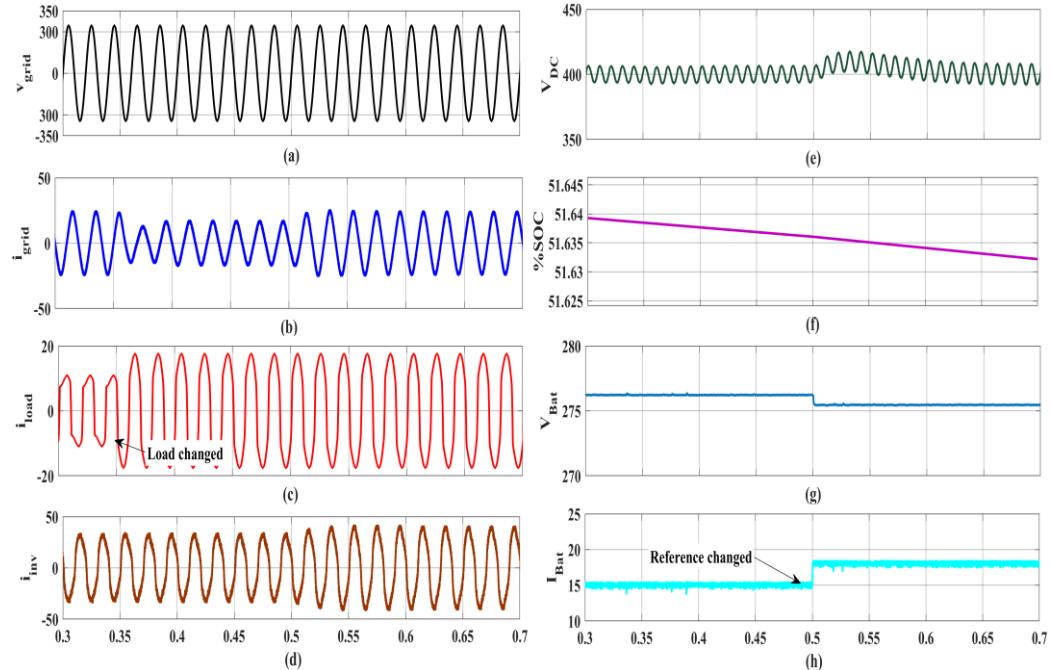


Fig. 4.8 V2G varying load and reference change, (a) v$_{grid}$ (b) i$_{grid}$ (c) i$_{load}$ (d) i$_{inverter}$ (e) V$_{DC}$ (f) %SOC (g) V$_{Bat}$ (h) I$_{bat}$

## 4.3.3 V2G with load and current reference variation

In this mode the battery in the vehicle supplies the load and the surplus energy is fed into the grid. Fig.4.8 shows the discharging of the battery at 15A current. Fig.4.8.(h)

28

represents that the discharging current remains constant irrespective of change in the load. Here the load is changed at t = 0.35s. It is clear from the Fig.4.8.(a)-4.8.(d) that when the load is increased the amount of current going into the grid decreases but the inverter current that depends upon current from the battery remains unaffected. The Simulink model is well developed to work at other specified current value. Here the reference current for battery discharging is varied from 15A to 18A at t = 0.5s and as observed from the Fig.4.8.(h) the model follows the change in reference value. Now as the discharging current is increased and the load remains constant the current being fed to the grid increases Fig.4.8.(b).

# Conclusion

Modelling and simulation of an on-board bidirectional EV charger has been discussed in this thesis. The bi-directional charging is obtained via using two converters one being AC-DC bi-directional converter the other is DC-DC converter. The bidirectional buck and boost converter is controlled to operate the EV battery in G2V and V2G modes. Only the output current (battery current) of bidirectional battery side DC-DC buck and boost converter is found to be continuous. A SOGI controller has been used to control the grid side converter. Simulink results verifies the desired operation in both the modes.

# Chapter 5

# Performance Evaluation of Buck and Boost Converter under Distorted Grid Condition

## 5.1 System Description

Fig.5.1 represents the basic schematic of the model. There are two power converters shown in the model. One is the grid side bidirectional ac-dc converter and the other one is dc-dc bidirectional EV-battery side converter. The dc bus is the common link between both the converters. A linear load ($R_L$) is also considered on the grid side.

The working of the proposed model can be studied in two modes discussed below in detail.

The Grid-to-EV-battery (or G2V) mode is first mode. In this mode, the grid supplies the energy to the load as well as the EV-battery. The power transfer can be explained as follows. The load is supplied by single-phase grid. The ac voltage is converted to dc voltage with the implementation of bidirectional ac-dc grid side converter which acts as a rectifier in this mode, converting the grid voltage into desired dc bus voltage.

After the dc bus there is another power converter circuit as shown in Fig.5.1. This converter circuit represents bidirectional dc-dc converter which steps up or steps down the dc bus voltage. In Grid-to-Ev-battery mode this bidirectional dc-dc converter acts as a buck converter. This buck converter steps down the dc bus voltage (400V) and regulates it to desired EV-battery voltage rating of 280V.

The second mode considered is the vehicle to grid mode (V2G). Here the power is transferred from the EV-battery to the load and grid. This power transfer is also aided by two bidirectional converters which are dc-dc bidirectional EV-battery side converter and the ac-dc bidirectional grid side converter. Here the bidirectional dc-dc converters work as a boost converter boosting the voltage from EV-battery level of 280V to the common dc bus voltage level of 400V. The second power converter is the bidirectional grid side ac-dc converter. In this mode this converter acts as an inverter converting the dc bus voltage to ac grid voltage. This converter distributes the energy from the EV-battery to the load and the surplus energy is then given to the grid.

The converter's control strategies are discussed in detail. There are two controllers for each of the converters and the designed control algorithm is studied in the following sub-sections.

30
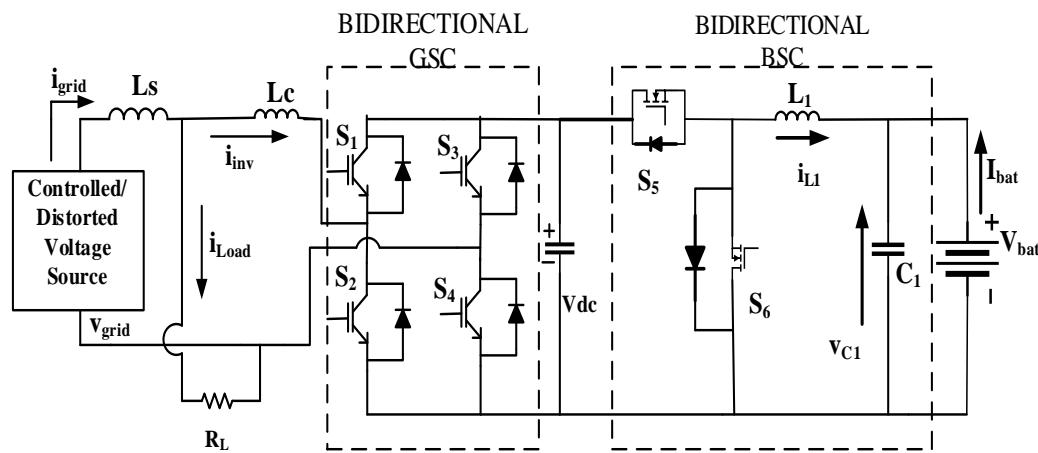
Fig.5.1. Complete system diagram with both the bidirectional converters.

## 5.2 Converter Control

in this section the converter control is explained.

### 5.2.1 EV-Battery side converter control

Since the EV-Battery side converter in this model is the same as in chapter 4, the control technique remains the same. Hence to avoid repetition the buck and boost control is not re-written here.

### 5.2.2 Grid side converter control

Unlike the previous control here we use two SOGI controller. One of the SOGI is used to generate the $I_{tot}$ as in chapter 4. The other one is use to generate the unit template.

The unit template control strategy is commonly used in AC-DC converters to regulate the output voltage and improve power quality. It works by extracting a reference signal from the input AC voltage, which is then used to generate a controlled switching pattern for the bidirectional AC-DC converter. This method helps in achieving power factor correction (PFC) and reducing harmonics in the system.

For EV chargers, unit template control is particularly useful in bidirectional charging systems (G2V and V2G modes). It helps in:

- **Grid synchronization** by ensuring the charger draws current in phase with the grid voltage.

- **Battery charging optimization**, ensuring controlled charging and discharging cycles.

- **Bidirectional energy flow**, allowing EVs to supply power back to the grid when needed.

31

- **Power quality improvement** by reducing harmonic distortion at the point of common coupling (PCC).

As shown in figure 5.2 the SOGI PLL is used to generate the two orthogonal components i.e $v_{alpha}$ and $v_{beta}$. The working and designing of SOGI are already discussed in chapter 4. Figure 5.3 shows how to obtain the Unit Template from obtained $v_{alpha}$ and $v_{beta}$.
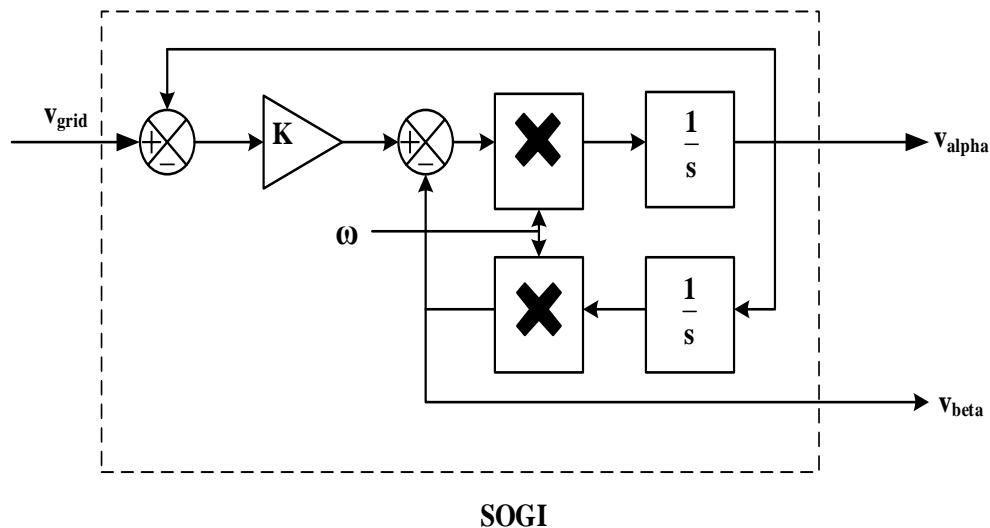


Fig.5.2. Generation of $v_{alpha}$ and $v_{beta}$ from SOGI -PLL
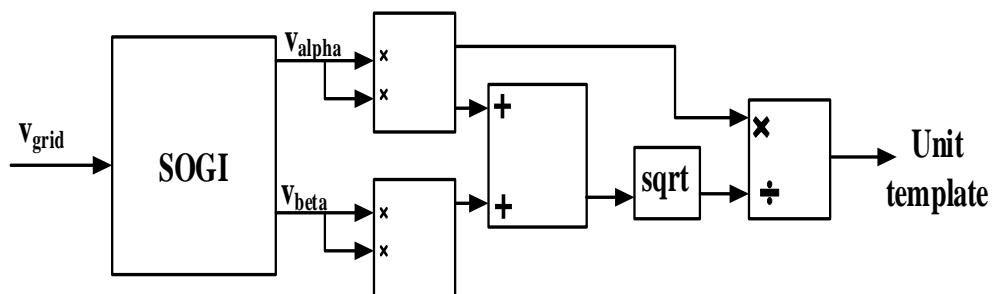


Fig. 5.3. Method to obtain unit template

The Unit Template (UT) is obtained using equation 5.1.

$$UT = \frac{V_{alpha}}{\sqrt{V_{alpha}^2 + V_{beta}^2}} \tag{5.1}$$

This UT is multiplied with $I_{total}$ to obtain reference signal $I_{ref}$, as shown in equation 5.2, which is compared with the grid current to generate the switching pulses as in figure 5.4.

32
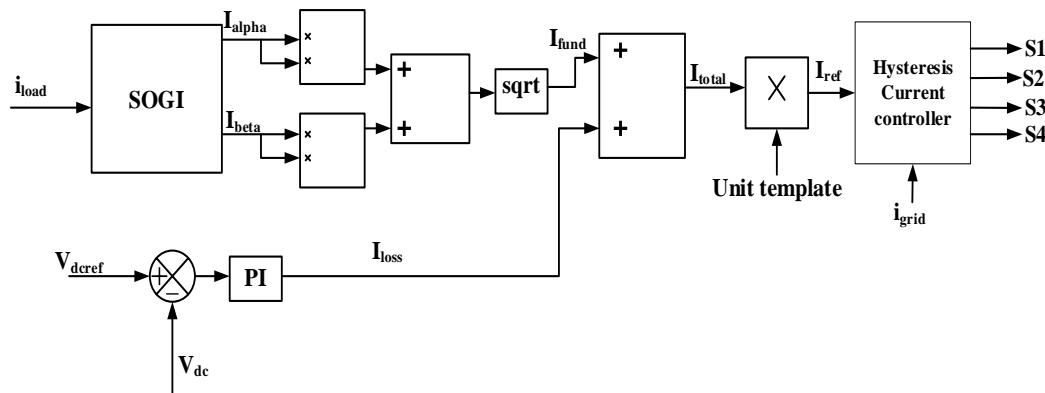
Fig. 5.4.  Complete control of grid side converter

$$I_{ref} = I_{total} * UT \tag{5.2}$$

## 5.3 Results Analysis

The results section is studied in two modes viz. charging as well as discharging. The first section depicts the charging of the EV-battery. The direction of power flow is from grid to EV-battery via bidirectional ac to dc converter and bidirectional dc to dc converter. The grid in this case supplies energy to the load and the EV-battery.

The second section depicts the discharging of the EV-battery. The power flow is reversed this time, from EV-battery to the grid as well as to the load. Stored energy in the battery is dissipated in the load and surplus energy (if any) is given to the grid.

Results in each of the modes are shown and discussed in detail.

### 5.3.1 Charging Mode:

Results for this mode are shown by Fig.5.5 and can be studied in five parts in different durations.

*A. Duration 1: 0.2s < t < 0.3s*

In this duration normal charging operation is shown. As grid is supplying power to the load, we can observe that the grid voltage and grid current are in the same phase as in Fig.5.5.(a,b). It can be observed that the grid current and grid voltage are purely sinusoidal. The current in the bidirectional ac-dc grid side converter is also maintained sinusoidal Fig.5.5.(d). The DC bus voltage is maintained at 400V Fig.5.5.(e), EV-

33
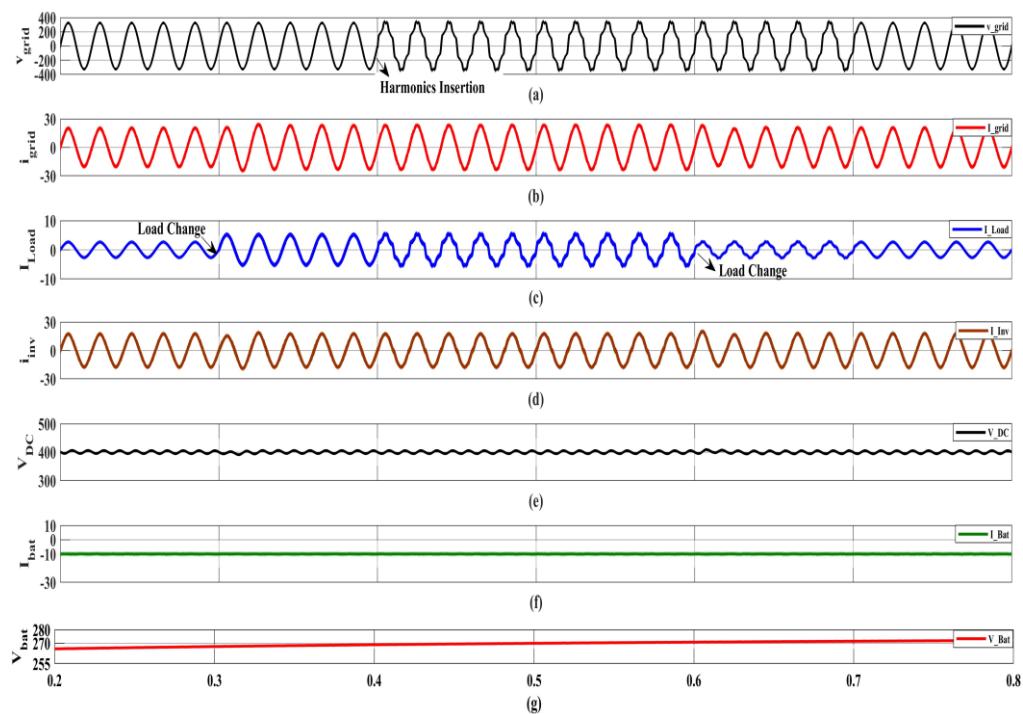
Fig. 5.5. Charging mode waveforms with buck & boost converter (a) $v_{grid}$, (b) $i_{load}$ (c) $I_{load}$ (d) $i_{inv}$ (e) $V_{DC}$ (f) $I_{bat}$ (g) $V_{bat}$

battery charging current is 10A as in Fig. 5.5.(f) (negative current represents charging of battery) and the battery is getting charged.

*B. Duration 2: 0.3s < t < 0.4s*

In this duration, load change condition is studied when grid is normal i.e. no harmonics are present in the grid side. Within this duration, Fig.5.5 shows clearly that as load is increased the grid current drawn from the grid has increased. Though the grid current and load current have changed, the charging current for the EV-battery remains unaffected and is constant at 10A. The DC link voltage is regulated to 400V which is the selected reference value. This suggests that our system is operating under desirable condition.

*C. Duration 3: 0.4s < t < 0.6s*

In this duration, the harmonics effects in grid voltage are considered. The harmonics effects are realized by using a programmable supply with harmonics injected into the grid. At t = 0.4s, the harmonics injected into the grid can be observed from Fig.5.5. The grid voltage becomes distorted at t = 0.4s due to the effect of harmonics at the grid side. From the figure it can also observed that these harmonics also flow into the load as load current also becomes distorted at this instant. But it can be observed that these harmonics don't distort the grid current and EV-battery charging current. This is due to the designed SOGI controller which acts as a phase locked loop as well as for reference current generation. It can be observed from Fig. 5.5.(b). that the grid side

34

AC-DC Bidirectional converter current remains pure sinusoidal. Thus, harmonics do not mitigate into the grid current as well as EV-battery charging current. EV-battery charging current also remains unaffected or undistorted from the effects of grid side harmonics as there is no distortions seen in the EV-battery charging current waveform of the Fig. 5.5.(f).

*D. Duration 4: 0.6s < t < 0.7s*

During this duration, performance of the system is verified under load variations. It can be observed from Fig. 5.5(a) that waveform of grid voltage "$v_{grid}$" is still distorted. Since the load is decreased the current from the grid current also decreases. This can be verified from the grid current waveform "$i_{grid}$" and load current waveform "$i_{Load}$". This load change has no effect on EV-battery charging dynamics which is constant at -10A.

*E. Duration 5: 0.7s < t < 0.8s*

In this duration, the simulated harmonic effects are removed and the normal operating condition is restored. Thus, the grid voltage and grid current waveforms are sinusoidal and load current is sinusoidal as well. The current through the AC-DC bidirectional grid side converter is also sinusoidal. The battery is being charged with constant DC current of 10A without any distortions.

The performance study depicted from t=0.2s to t=0.8s depicts the system operation is stable irrespective of load change or harmonics on the grid side. The EV- battery charging current remains undisturbed due to disturbance on the grid side. The designed SOGI controllers are performing the control actions satisfactorily.

## 5.3.2 Discharging Mode

Performance results for this mode of operation are shown in Fig.5.6. The following sub-section gives detailed understanding of this mode under load changes and grid abnormalities.

*A. Duration 1: 0.2s < t < 0.3s*

In this duration, normal grid is considered and discharging operation is shown. As the EV-battery is supplying power to the load as well as to the grid, it can be observed that the grid voltage and grid current are in opposite phase. It can be observed that the grid voltage and grid current are purely sinusoidal. The current in the bidirectional ac-dc grid side converter is also maintained sinusoidal, this current is also in anti-phase to grid voltage which assures energy is being transferred from the EV-battery side to grid and load side. The DC bus voltage is maintained at 400V, EV-battery discharging current is 10A (the positive value of current indicates the current flowing out of the battery in other words battery is delivering the energy).

35

Fig. 5.6.  Discharging mode waveforms with buck & boost converter (a) $v_{grid}$, (b) $i_{load}$ (c) $I_{load}$ (d) $i_{inv}$ (e) $V_{DC}$ (f) $I_{bat}$ (g) $V_{bat}$

### B. Duration 2: 0.3s < t < 0.4s

In this duration, load change condition is simulated when grid is normal that is no harmonics are present in the grid voltage. During this duration, Fig. 5.6 depicts that as the load is increased (increased '$i_{Load}$') the grid current ('$i_{grid}$') decreases. This is because the discharging current from the EV-battery is constant DC at 10A flowing from the battery, as more current flows into the load, the current going into the grid decreases. This suggests that our system is operating under desirable conditions.

### C. Duration 3: 0.4s < t < 0.6s

In this subsection the harmonics effects in grid voltage are considered. The harmonics effects are realized by simulating harmonics into the grid. At t= 0.4s, the harmonics are injected to the grid as observed in Fig. 5.6. The effect of the harmonics can be observed in the grid voltage. The grid voltage becomes distorted at t=0.4s due to the effect of harmonics in the grid side. From the figure, it can also be observed that these harmonics also flow into the load as load current also becomes distorted at this instant. But, these harmonics don't distort the EV-battery discharging current ('$I_{Bat}$') and grid current ('$i_{grid}$') due to appropriate controller action. The results in Fig. 5.6 show that the grid current and grid side AC-DC Bidirectional converter current('$i_{inv}$') remains pure sinusoidal even under the influence of harmonics. EV-battery discharging current also remains unaffected or undistorted from the effects of grid side harmonics as there are no distortions seen in the EV-battery discharging current waveform of the Fig. 5.6.

36

*D. Duration 4: 0.6s < t < 0.7s*

This duration is to re-verify that system is operating in good desired condition if there are any load variations. As observed from the figure during 0.6s < t < 0.7s, the waveform of grid voltage "$v_{grid}$" shows the presence of distortions. Since the load is decreased the current going into the grid increases as the discharging current from the EV-battery is maintained constant at 10A. This can be verified from the grid current waveform '$i_{grid}$', load current waveform '$i_{Load}$' and EV-battery discharging current '$I_{Bat}$'.

*E. Duration 5: 0.7s < T < 0.8s*

In this duration, at t = 0.7s, the simulated harmonics effects are removed and the normal operating condition is restored. The grid voltage and grid current waveforms are sinusoidal as well in anti-phase and load current as well is sinusoidal. The current through the AC-DC bidirectional grid side converter is also sinusoidal. The battery is being discharged with constant DC current of 10A without any distortions.

During all the time durations from t=0.2s to t=0.8s, the developed system operation is stable irrespective of load change or harmonics on the grid side. The EV- battery discharging current remains undisturbed due to disturbance on the grid side. The DC link voltage is stabilized and regulated at 400V.

# CONCLUSION

A bidirectional on-board charger has been proposed in this paper. The control algorithm is based on SOGI control and it is developed such that the harmonic disturbances on the grid side are not reflected on the grid current as well as charging and discharging current of the battery. Design of SOGI controller is proposed for determining the fundamental current component as well as a phase locked loop. The simulated performance results have been shown for a bidirectional buck & boost converter as well as AC-DC bidirectional converter. Simulation studies are performed under load variations as well as grid abnormalities to verify the operation of the proposed model. The results show the effectiveness of the proposed controller in both the operating modes.

37

# Chapter 6

# Performance Analysis of Grid Connected EV Charger using Bidirectional Cuk Converter

## 6.1 System configuration

The suggested configuration is represented in Fig.6.1. The system is made up of two bidirectional converters, the first is Grid Side Converter (GSC) and the second is Battery Side Converter (BSC). Both the bidirectional converters interact with each other via a common DC link having DC link voltage of $V_{DC}$

In G2V mode, the bidirectional AC-DC grid side converter (GSC) feeds energy to the battery through a DC link capacitor by acting as a rectifier. On the other hand, in V2G mode the load is fed by the battery and the remaining energy is fed into the grid. A bidirectional Cuk converter is used to connect the DC link and the battery of the EV. The bidirectional Cuk converter can run in either of the two modes i.e., in buck or boost mode. In G2V mode, the DC-DC Cuk converter is utilized as to charge the battery at constant DC current, here the Cuk converter works in buck mode. The bidirectional Cuk converter operates in boost mode in V2G mode, supplying energy to the load and grid.
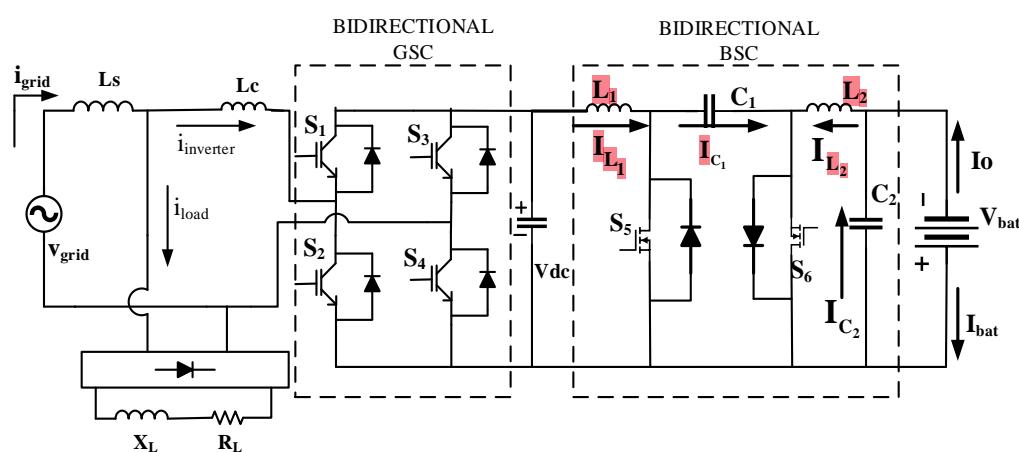


Fig.6.1 System configuration with cuk converter.

The battery with bidirectional BSC is connected at DC link of GSC. Further, the interfacing inductor Lc with GSC is connected at common point of the load and the grid.

38

## 6.2 controller design

Design of controller for Battery Side Converter and Grid Side Converter is discussed in this section.

### 6.2.1 BSC (Battery Side Converter)

*A. Charging mode*

In charging mode, the charging current of the BSC is controlled by controlling the current in inductor $L_1$ current ($I_{L1}$) as seen in Fig 6.2.(a). The average inductor current $I_{L1}$ is equal to the average current input to the converter. Therefore, $I_{L1}$ is calculated as follows.

Assuming efficiency to be 100%,

$$P_{in} = P_{out} \tag{6.1}$$

$$V_{dc} * I_{L1} = V_{bat} * I_o \tag{6.2}$$

$$I_{L1} = \frac{V_{bat} * I_o}{V_{dc}} \tag{6.3}$$

$I_{L1ref}$ is the reference current and is compared with the actual inductor current $I_{L1}$ to obtain an error signal. A PI controller receive this error. A comparator receives the PI controller's output along with triangular switching sequence at the frequency of 10 kHz. The, control scheme in charging mode is depicted in Fig. 3(a). The output of the comparator is used as the gating pulse for switch $S_5$ of the cuk converter and the negation of this signal is used as the gating pulse for switch $S_6$.
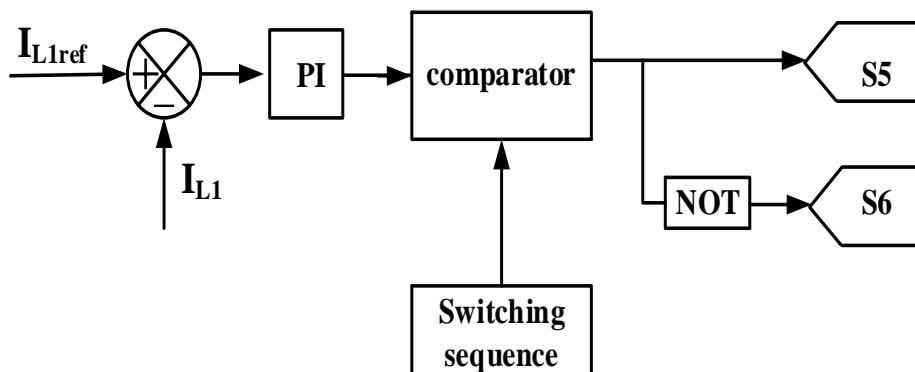


Fig. 6.2.(a). G2V (charging) mode control

*B. Discharging Mode*

The, control scheme in discharging mode is shown in Fig.6.2.(b). Battery current ($I_{bat}$) and the reference current ($I_{batref}$) are compared to get an error signal which is fed into

39

a PI controller. A comparator receives the PI controller's output along with carrier signal at the frequency of 10 kHz. The output of the comparator is used as the gating pulse for switch $S_5$ of the cuk converter and the negative of this signal is used as the gating pulse for switch $S_6$.
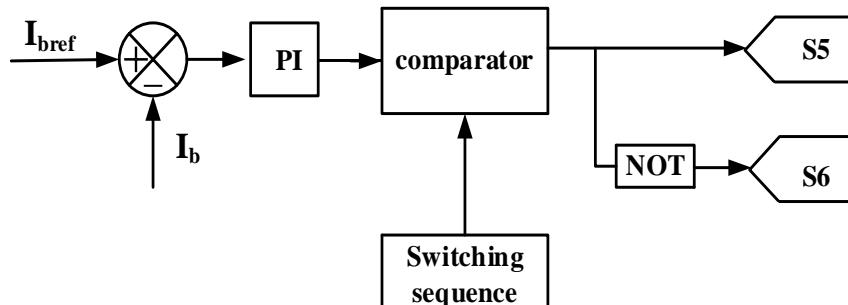


Fig. 6.2.(b). V2G (discharging) mode control

## 6.2.2 GSC (Grid Side Converter)

The control is similar to chapter 4, though a short discussion is done in this sub-section.
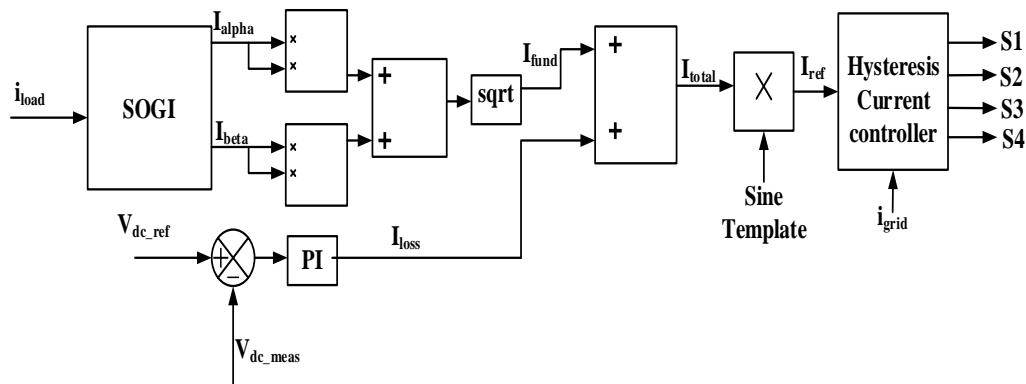


Fig. 6.3. Control for grid side converter

The switching pulses are generated from the hysteresis controller whose inputs are grid current $i_{grid}$ and reference current $i_{ref}$. The reference current is generated from the load current $i_{load}$. With the help of SOGI quadrature signal $I_{alpha}$ and $I_{beta}$ are generated. Then with the help of these signal fundamental current $I_{fund}$ is obtained as shown in the figure 6.3. This signal is added with the loss current $I_{loss}$ to consider the losses occurring in the bidirectional ac-dc GSC, to finally obtain the $I_{total}$. This signal is multiplied with a sine template which is generated using the grid voltage in order to maintain unity form factor.

40

## 6.3 Results analysis

A Simulink model is developed and analysis under G2V and V2G is tested. A detailed discussion is discussed in following sections:

### 6.3.1 Charging and Discharging mode

The Simulink model simulation results for grid voltage, grid current, load current, inverter current, voltage at DC bus, battery voltage, battery current, %SOC (State Of Charge), and current through inductor $L_1$ is shown in Fig.6.4, for both the modes G2V as well as V2G mode. The bidirectional cuk converter is designed for DC bus voltage of 400V, battery rating is selected as 280V, 25Ah.
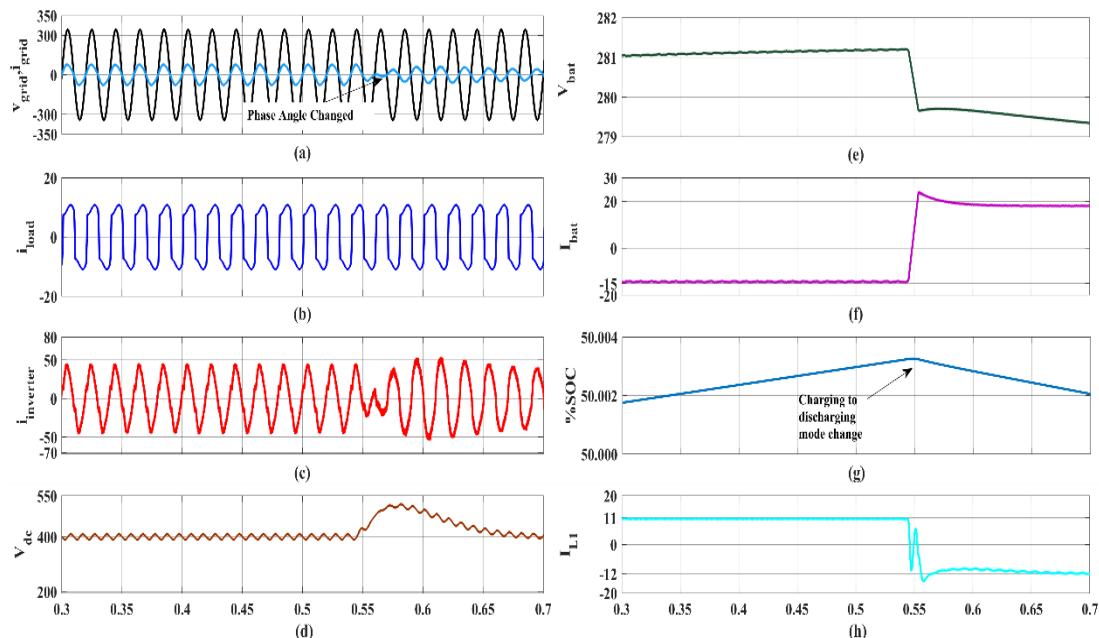


Fig. 6.4. Charging and discharging modes of operation (a) $v_{grid}$, $i_{grid}$ (b) $i_{load}$ (c) $i_{inverter}$ (d) $V_{dc}$ (e) $V_{bat}$ (f) $I_{bat}$ (g) %SOC (h) $I_{L1}$

As seen from Fig. 6.4.(a) the grid voltage and grid current are in same phase in charging *i.e.,* G2V mode which states that power is being supplied from grid to battery. Also, at some instant (t=0.55s) the model is made to operate in V2G *i.e.,* battery discharging mode. It can from Fig. 6.4.(a) that the grid current is now in phase opposition to grid voltage, which states that battery is supplying current to the grid, hence the energy flow occurs from battery to grid. Also, while charging (from time t = 0s to time t = 0.55s) the battery current is negative Fig.6.4.(f) which is an indicator of battery being charged on the other hand while discharging (from time t = 0.55s to time t = 0.7s) the battery current is positive. Fig.6.4.(f) shows battery is being discharged and the battery current is continuous in nature.

41
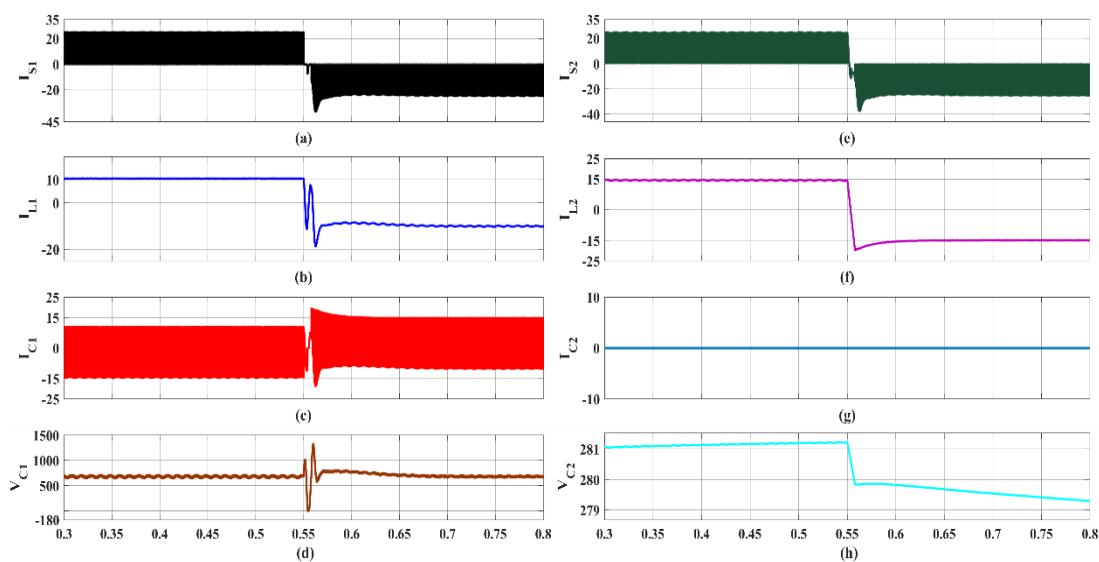
Fig.6.5. Plots of different elements of cuk converter (a)$I_{S1}$ (b)$I_{L1}$ (c)$I_{C1}$ (d)$V_{C1}$ (e)$I_{S2}$ (f)$I_{L2}$ (g)$I_{C2}$ (h) $V_{C2}$

Fig.6.5.(a)-(h) shows the waveforms for different elements present in the bidirectional cuk converter. Fig. 6.5(b) indicates almost negligible ripple in input source side current. From Fig6.5(f, g) we can say that the current in the output has less ripple. That is ripple on both the input and output is very less and hence the filter requirement for the converter is small and less expensive. Fig. 6.5(b) shows that the DC side current which is input to the Cuk converter is continuous.

This is in contrast to the input current of the DC-DC buck and boost converter used earlier in chapter 4. As seen from the Fig.6.5 the input current is discontinuous in nature. This demands for a filter at the input side of the buck and boost converter.
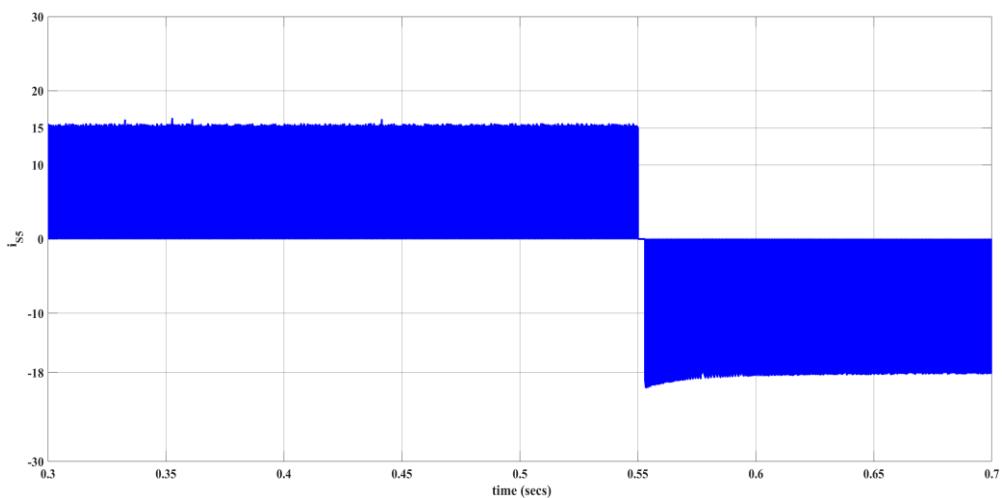


Fig.6.6. Input current waveform of the buck and boost converter in charging and discharging mode.

42

## 6.3.2 G2V with load and current reference variation

The model is designed to charge the battery with 15 A current. In the Fig.6.7, the load is changed at t = 0.35s, the Fig. 6.7.(f) shows even if there are load changes the designed model can still charge the battery at designed value of current. Increasing the load increases the power demand from the grid as a result more current is drawn, from the grid, also changing the load should not affect the charging current of the battery, both of these statements are verified from the Fig.6.7.(a)-6.7.(c), 6.7.(f). Fig. 6.7.(f)-6.7.(h) also illustrate that the designed model can also perform well if battery is required to charge at other current level. Here the battery reference is varied from 15A to 18A at t = 0.5s. Increasing the battery charging reference current increases the current drawn from the grid which is also reflected as increased inverter current Fig. 6.7.(c). The battery current is controlled indirectly via controlling the current in the first inductor ($L_1$) of the bidirectional Cuk converter. Therefore, the inductor current ($I_{L1}$) is changed from 10.5A to 12.6A (this value is calculated using equation 6.3) as shown in Fig.6.7.(h).
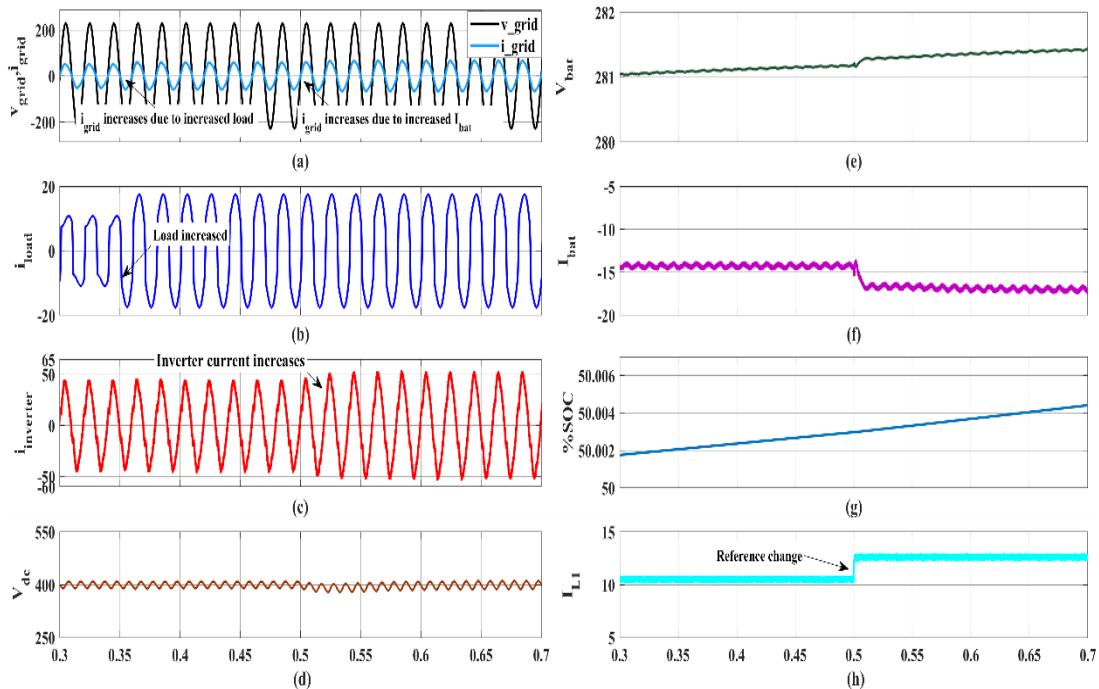


Fig. 6.7. G2V varying load & reference change, (a) $v_{grid}$,$i_{grid}$ (b) $i_{load}$ (c) $i_{inverter}$ (d)$V_{dc}$ (e) $V_{bat}$ (f) $I_{bat}$ (g) %SOC (h) $I_{L1}$

43

### 6.3.3 V2G with load and current reference variation

In this mode the battery in the vehicle supplies the load and the surplus energy is fed into the grid. Fig.6.8 shows the discharging of the battery at 15A current. Fig.6.8(f) represents that the discharging current remains constant irrespective of change in the load. Here the load is changed at t = 0.35s. It is clear from the Fig. 6.8(a)-6.8(c) that when the load is increased the amount of current going into the grid decreases but the inverter current that depends upon current from the battery remains unaffected. The Simulink model is well developed to work at other specified current value. Here the reference current for battery is varied from 15A to 18A at t = 0.5s and as observed from the Fig.6.8.(f) the model follows the change in reference value. Now when discharging current is increased since, the load is constant the current being fed to the grid increases Fig.6.8s.(a).
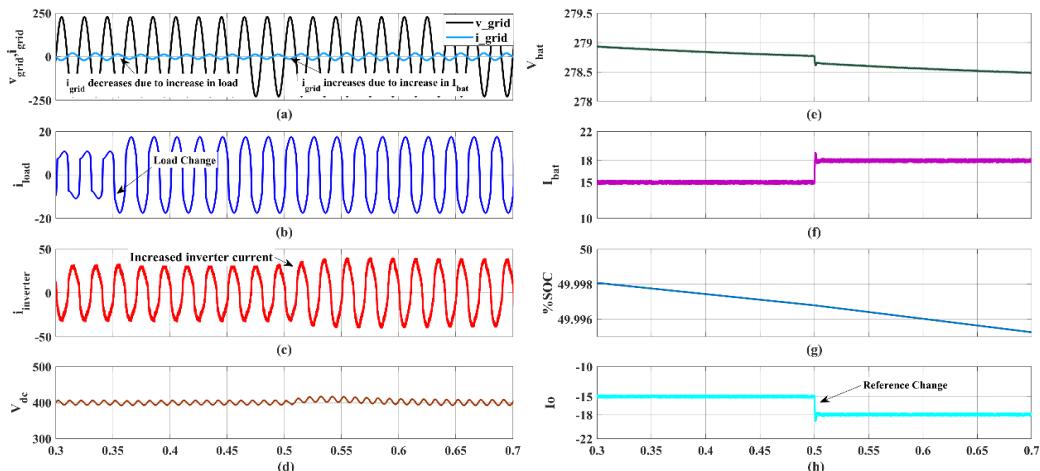


Fig. 6.8.V2G varying load & reference change, (a) $v_{grid}$, $i_{grid}$ (b) $i_{load}$ (c) $i_{inverter}$ (d) $V_{dc}$ (e) $V_{bat}$ (f) $I_{bat}$ (g) %SOC (h) $I_o$

## Conclusion

Modelling and simulation of an on-board bidirectional EV charger has been discussed in this thesis. The bi-directional charging is obtained via using two converters one being AC-DC bi-directional converter the other is DC-DC converter. The bidirectional cuk converter is controlled to operate the EV battery in G2V and V2G modes. Both input and output current of bidirectional battery side Cuk converter is found to be continuous (in contrast to the input current waveform of buck and boost converter, where the current is discontinous). SOGI controller have been used to control the grid side converter. Simulink results verify the desired operation in both the modes.

# Chapter 7

## Performance Evaluation of Cuk Converter under Distorted Grid Condition

## 7.1 System Description

Fig.7.1 represents the basic schematic of the model. There are two power converters present in the model. One is the grid side bidirectional ac-dc converter (GSC) and the other one is dc-dc bidirectional EV-battery side converter (BSC). The dc bus is the common link between both the converters. A linear load ($R_L$) is also considered on the grid side.

The working is similar to that explained in chapter 5. The difference being that the DC-DC bidirectional buck and boost converter is replaced via a DC-DC bidirectional Cuk converter in this study.
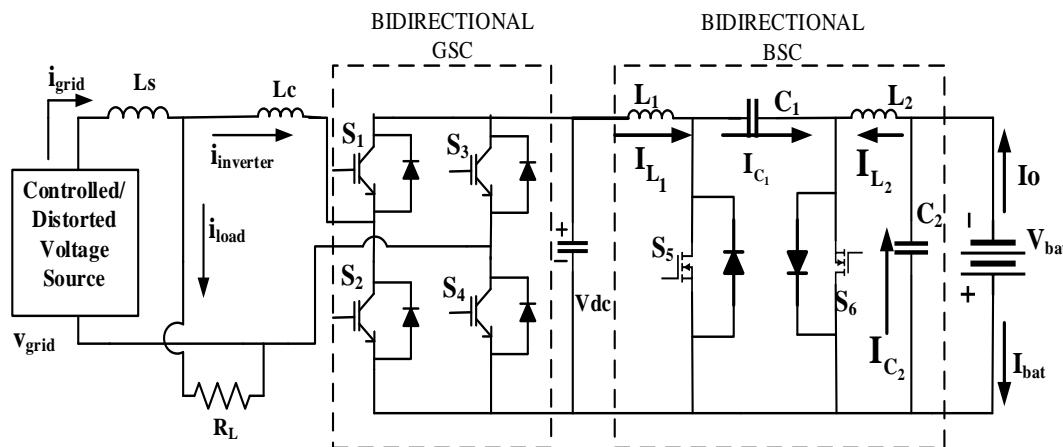


Fig.7.1 Proposed system for studying distorted grid effect with cuk converter

The polluted grid block contains of harmonics which use to simulate distorted grid condition. The effect of this block is controlled via the switch $S_g$. This switch is ON in the interval t = 0.4 to t = 0.7.

## 7.2 Controller Working

There are two controller one each for each of the bidirectional converters.

### 7.2.1 BSC (battery side converter)

The control algorithm for the BSC *i.e* bidirectional cuk converter is same as discussed in chapter 6 under the sub heading 6.2.1. In this chapter only the operating condition differs from the chapter 6 and hence the output current reference ($I_o$) while discharging, and the input inductor current ($I_{L1}$) while charging changes. Here the battery current is

45

kept at an absolute value of 10Amps both while charging and discharging. Therefore, while charging the input inductor current reference is set to $I_{L1}$=10. Which is calculated from the equation 6.3

$$I_{L1ref} = \frac{V_{bat}*I_o}{V_{dc}} \qquad \text{(from eq 6.3)}$$

$$I_{L1ref} = \frac{280*10}{400} = 7A \qquad (7.1)$$

And, while discharging the reference output current is set to $I_{0ref}$= -10A.

## 7.2.2 Grid side converter (GSC)

The grid side converter remains the same as in chapter 5 and though for a fast recall it is shortly discussed here.

# 7.3 Result Analysis

The results section is studied in two modes viz. charging as well as discharging. The first section depicts the charging of the EV- battery. The direction of power flow is from grid to EV-battery via bidirectional ac to dc converter and bidirectional dc to dc converter. The grid in this case supplies energy to the load and the EV-battery.

The second section depicts the discharging of the EV-battery. The power flow is reversed this time, from EV-battery to the grid as well as to the load. Stored energy in the battery is dissipated in the load and surplus energy (if any) is given to the grid.

Results in each of the modes are shown and discussed in detail.

## 7.3.1 Charging Mode

Results for this mode are shown by Fig.7.2 and can be studied in five parts in different durations.

*A. Duration 1: 0.2s < t < 0.3s*

In this duration normal charging operation is shown. As grid is supplying power to the load, we can observe that the grid voltage and grid current are in the same phase as in Fig.7.2.(a,b). It can be observed that the grid current and grid voltage are purely sinusoidal. The current in the bidirectional ac-dc grid side converter is also maintained sinusoidal Fig. 7.2.(d). The DC bus voltage is maintained at 400V Fig. 7(e), EV-battery charging current is 10A as in Fig.7.2.(f) (negative current represents charging of battery) and the battery is getting charged.
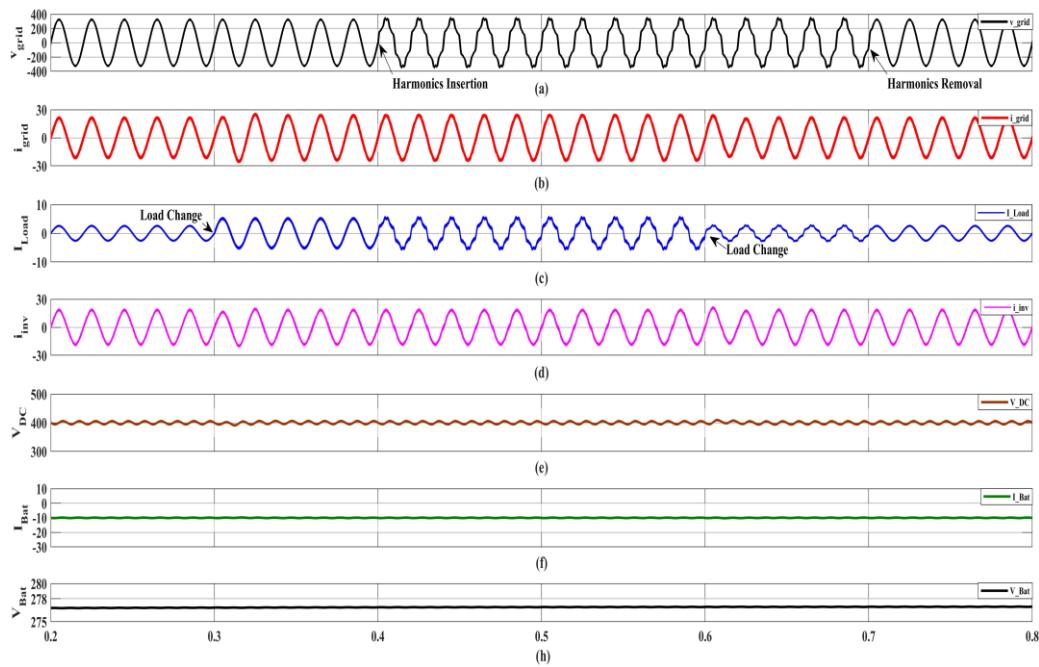
Fig.7.2. Charging condition waveform with cuk converter (a) $v_{grid}$, (b) $i_{load}$ (c) $I_{load}$ (d) $i_{inv}$ (e) $V_{DC}$ (f) $I_{bat}$ (g) $V_{bat}$

### B. Duration 2: 0.3s < t < 0.4s

In this duration, load change condition is studied when grid is normal i.e. no harmonics are present in the grid side. Within this duration, Fig.7.2 shows clearly that as load is increased the grid current drawn from the grid has increased. Though the grid current and load current have changed, the charging current for the EV-battery remains unaffected and is constant at 10A. The DC link voltage is regulated to 400V which is the selected reference value. This suggests that our system is operating under desirable condition.

### C. Duration 3: 0.4s < t < 0.6s

In this duration, the harmonics effects in grid voltage are considered. The harmonics effects are realized by using a programmable supply with harmonics injected into the grid. At t = 0.4s, the harmonics injected into the grid can be observed from Fig.7.2. The grid voltage becomes distorted at t = 0.4s due to the effect of harmonics at the grid side. From the figure it can also observed that these harmonics also flow into the load as load current also becomes distorted at this instant. But it can be observed that these harmonics don't distort the grid current and EV-battery charging current. This is due to the designed SOGI controller which acts as a phase locked loop as well as for reference current generation. It can be observed from Fig.7.2.(b). that the grid side AC-DC Bidirectional converter current remains pure sinusoidal. Thus, harmonics do not mitigate into the grid current as well as EV-battery charging current. EV-battery charging current also remains unaffected or undistorted from the effects of grid side

47

harmonics as there is no distortions seen in the EV-battery charging current waveform of the Fig.7.2.(f).

### D. Duration 4: 0.6s < t < 0.7s

During this duration, performance of the system is verified under load variations. It can be observed from Fig.7.2.(a) that waveform of grid voltage "$v_{grid}$" is still distorted. Since the load is decreased the current from the grid current also decreases. This can be verified from the grid current waveform "$i_{grid}$" and load current waveform "$i_{Load}$". This load change has no effect on EV-battery charging dynamics which is constant at -10A.

### E. Duration 5: 0.7s < t < 0.8s

In this duration, the simulated harmonic effects are removed and the normal operating condition is restored. Thus, the grid voltage and grid current waveforms are sinusoidal and load current is sinusoidal as well. The current through the AC-DC bidirectional grid side converter is also sinusoidal. The battery is being charged with constant DC current of 10A without any distortions.

The performance study depicted from t=0.2s to t=0.8s depicts the system operation is stable irrespective of load change or harmonics on the grid side. The EV- battery charging current remains undisturbed due to disturbance on the grid side. The designed SOGI controllers are performing the control actions satisfactorily.

## 7.2.2 Discharging Mode

Performance results for this mode of operation are shown in Fig.7.3. The following sub-section gives detailed understanding of this mode under load changes and grid abnormalities.

### A. Duration 1: 0.2s < t < 0.3s

In this duration, normal grid is considered and discharging operation is shown. As the EV-battery is supplying power to the load as well as to the grid, it can be observed that the grid voltage and grid current are in opposite phase. It can be observed that the grid voltage and grid current are purely sinusoidal. The current in the bidirectional ac-dc grid side converter is also maintained sinusoidal, this current is also in anti-phase to grid voltage which assures energy is being transferred from the EV-battery side to grid and load side. The DC bus voltage is maintained at 400V, EV-battery discharging current is 10A (the positive value of current indicates the current flowing out of the battery in other words battery is delivering the energy).

### B. Duration 2: 0.3s < t < 0.4s

In this duration, load change condition is simulated when grid is normal that is no harmonics are present in the grid voltage. During this duration, Fig.7.3.(b) & Fig.7.3.(c) depicts that as the load is increased (increased '$i_{Load}$') the grid current

48

('i_grid') decreases. This is because the discharging current from the EV-battery is constant DC at 10A flowing from the battery, as more current flows into the load, the current going into the grid decreases. This suggests that our system is operating under desirable conditions.
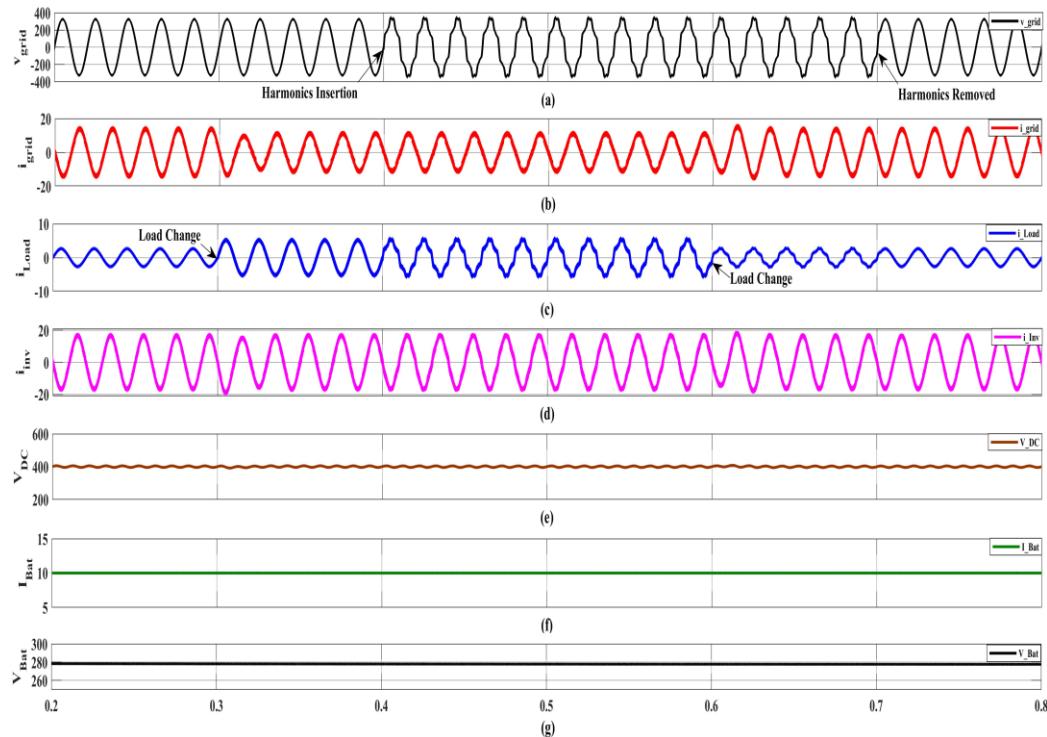


Fig.7.3 Disharging condition waveform with cuk converter (a) $v_{grid}$, (b) $i_{load}$ (c) $I_{load}$ (d) $i_{inv}$ (e) $V_{DC}$ (f) $I_{bat}$ (g) $V_{bat}$

### C. Duration 3: 0.4s < t < 0.6s

In this subsection the harmonics effects in grid voltage are considered. The harmonics effects are realized by simulating harmonics into the grid. At t = 0.4s, the harmonics are injected to the grid as observed in Fig.7.3.(a). The effect of the harmonics can be observed in the grid voltage. The grid voltage becomes distorted at t=0.4s due to the effect of harmonics in the grid side. From the figure, it can also be observed that these harmonics also flow into the load as load current also becomes distorted at this instant. But, these harmonics don't distort the EV-battery discharging current ('I_Bat') and grid current ('i_grid') due to appropriate controller action. The results in Fig.7.3.(b) & (c) show that the grid current and grid side AC-DC Bidirectional converter current('i_inv') remains pure sinusoidal even under the influence of harmonics. EV-battery discharging current also remains unaffected or undistorted from the effects of grid side harmonics as there are no distortions seen in the EV-battery discharging current waveform of the Fig.7.3.

49

### D. Duration 4: 0.6s < t < 0.7s

This duration is to re-verify that system is operating in good desired condition if there are any load variations. As observed from the figure during 0.6s < t < 0.7s, the waveform of grid voltage "$v_{grid}$" shows the presence of distortions. Since the load is decreased the current going into the grid increases as the discharging current from the EV-battery is maintained constant at 10A. This can be verified from the grid current waveform '$i_{grid}$', load current waveform '$i_{Load}$' and EV-battery discharging current '$I_{Bat}$'.

### E. Duration 5: 0.7s < T < 0.8s

In this duration, at t = 0.7s, the simulated harmonics effects are removed and the normal operating condition is restored. The grid voltage and grid current waveforms are sinusoidal as well in anti-phase and load current as well is sinusoidal. The current through the AC-DC bidirectional grid side converter is also sinusoidal. The battery is being discharged with constant DC current of 10A without any distortions.

During all the time durations from t = 0.2s to t = 0.8s, the developed system operation is stable irrespective of load change or harmonics on the grid side. The EV- battery discharging current remains undisturbed due to disturbance on the grid side. The DC link voltage is stabilized and regulated at 400V.

# CONCLUSION

A bidirectional on-board charger has been proposed in this paper. The control algorithm is based on SOGI control and it is developed such that the harmonic disturbances on the grid side are not reflected on the grid current as well as charging and discharging current of the battery. Design of SOGI controller is proposed for determining the fundamental current component as well as a phase locked loop. The simulated performance results have been shown for a bidirectional buck & boost converter as well as AC-DC bidirectional converter. Simulation studies are performed under load variations as well as grid abnormalities to verify the operation of the proposed model. The results show the effectiveness of the proposed controller in both the operating modes.

To summarize the comparison between both the converters has been provided in the following table:

50

Table III: Comparison between bidirectional DC-DC converters

| S.No | Parameter | Bidirectional Ćuk Converter | Bidirectional Buck-Boost Converter |
|------|-----------|------------------------------|-------------------------------------|
| 1. | Topology | Utilizes two inductors, one capacitor for energy transfer | Single inductor topology |
| 2. | Energy Transfer | Energy is transferred via a capacitor | Energy is transferred via inductor |
| 3. | Voltage Polarity | Output voltage is **inverted** (opposite polarity to input) | Output voltage is **non-inverted** |
| 4. | Continuous Input/Output Current | Yes – due to presence of inductors on both sides | No – output or input current may be discontinuous |
| 5. | Component Count | Higher – requires two inductors and one coupling capacitor | Lower – requires one inductor |
| 6. | Efficiency | Moderate – increased losses due to more components and coupling capacitor | Generally higher due to fewer components and reduced conduction paths |
| 7. | Voltage Gain Range | Wide – can operate in buck, boost, and buck-boost modes | Also wide – operates in buck-boost mode |
| 8. | Control Complexity | More complex due to coupling capacitor and continuous conduction requirement | Relatively simple |
| 9. | Size and Weight | Larger – more passive components | Compact – fewer components |
| 10. | Ripple Characteristics | Lower input and output current ripple | Higher ripple, especially in output current |
| 11. | EMI (Electromagnetic Interference) | Lower – continuous currents reduce EMI | Higher – discontinuous current leads to increased EMI |
| 12. | Stress on Components | Stress shared across components (but added capacitor voltage stress) | Switches endure full load current and voltage stress |

51

| 13. | Cost | Higher – due to additional passive components | Lower – minimal components |
|---|---|---|---|
| 14. | Bidirectional Control | Supports power flow in both directions, with proper switch control | Supports bidirectional operation with proper control |
| 15. | Suitability for EV Applications | Better suited for applications where ripple current must be minimized | Suitable for simpler EV charging systems with size/efficiency constraints |

# REFERENCES

[1] Manojlović, A. V., Medar, O. M., Anđelković, A. S., & Tomić, M. A. (2023). Environmental impact assessment of the electric vehicles: A case study. *Energy Sources, Part A: Recovery, Utilization, and Environmental Effects*, *45*(1), 1007–1016.

[2] Shah, R. V. (2022). Financial incentives for promotion of electric vehicles in India-An analysis using the environmental policy framework. *Nature Environment and Pollution Technology*, *21*(3), 1227-1234.

[3] Chaturvedi, B. K., Nautiyal, A., Kandpal, T. C., & Yaqoot, M. (2022). Projected transition to electric vehicles in India and its impact on stakeholders. *Energy for Sustainable Development*, *66*, 189-200.

[4] Rather, Z., Banerjee, R., Nath, A., & Dahiwale, P. (2021). Fundamentals of electric vehicle charging technology and its grid integration. *Nationally Determined Contributions-Transport Initiative for Asia (NDC-TIA)*.

[5] Mal, S., Chattopadhyay, A., Yang, A., & Gadh, R. (2012). Electric vehicle smart charging and vehicle-to-grid operation. *International Journal of Parallel, Emergent and Distributed Systems*, *28*(3), 249–265.

[6] Sagaria, Shemin, Mart van der Kam, and Tobias Boström. "Vehicle-to-grid impact on battery degradation and estimation of V2G economic compensation." *Applied Energy* 377 (2025): 124546.

[7] M. Yilmaz and P. T. Krein, "Review of benefits and challenges of vehicle-to-grid technology," 2012 IEEE Energy Conversion Congress and Exposition (ECCE), Raleigh, NC, USA, 2012, pp. 3082-3089, doi: 10.1109/ECCE.2012.6342356.

[8] H. Wouters and W. Martinez, "Bidirectional Onboard Chargers for Electric Vehicles: State-of-the-Art and Future Trends," in IEEE Transactions on Power Electronics, vol. 39, no. 1, pp. 693-716, Jan. 2024, doi: 10.1109/TPEL.2023.3319996.

[9] Lipu MSH, Faisal M, Ansari S, Hannan MA, Karim TF, Ayob A, Hussain A, Miah MS, Saad MHM. Review of Electric Vehicle Converter Configurations, Control Schemes and Optimizations: Challenges and Suggestions. *Electronics*. 2021; 10(4):477.

[10] Chakraborty S, Vu H-N, Hasan MM, Tran D-D, Baghdadi ME, Hegazy O. DC-DC Converter Topologies for Electric Vehicles, Plug-in Hybrid Electric Vehicles and Fast Charging Stations: State of the Art and Future Trends. *Energies*. 2019; 12(8):1569.

[11] Heydari-doostabad, Hamed, and Terence O'Donnell. "A wide-range high-voltage-gain bidirectional DC–DC converter for V2G and G2V hybrid EV charger." *IEEE Transactions on Industrial Electronics* 69.5 (2021): 4718-4729.

53

[12] Cuk, Slobodan, and R. D. Middlebrook. "A new optimum topology switching DC-to-DC converter." *1977 IEEE Power Electronics Specialists Conference*. IEEE, 1977.

[13] Duran, E., Sidrach-de-Cardona, M., Galan, J., & Andujar, J. M. (2008, June). Comparative analysis of buck-boost converters used to obtain I–V characteristic curves of photovoltaic modules. In *2008 IEEE Power Electronics Specialists Conference* (pp. 2036-2042). IEEE.

[14] Seguel JL, Seleme SI Jr., Morais LMF. Comparative Study of Buck-Boost, SEPIC, Cuk and Zeta DC-DC Converters Using Different MPPT Methods for Photovoltaic Applications. *Energies*. 2022; 15(21):7936.

[15] Zgheib, R., Al-Haddad, K., & Kamwa, I. (2016, March). V2G, G2V and active filter operation of a bidirectional battery charger for electric vehicles. In *2016 IEEE International Conference on Industrial Technology (ICIT)* (pp. 1260-1265). IEEE

[16] Verma, Anjeet, and Bhim Singh. "AFF-SOGI-DRC control of renewable energy based grid interactive charging station for EV with power quality improvement." *IEEE Transactions on Industry Applications* 57.1 (2020): 588-597.

[17] Hu, Kai-Wei, Pei-Hsun Yi, and Chang-Ming Liaw. "An EV SRM drive powered by battery/supercapacitor with G2V and V2H/V2G capabilities." *IEEE transactions on industrial electronics* 62.8 (2015): 4714-4727.

[18] Kumar, Gangavarapu Guru, and Kumaravel Sundaramoorthy. "Dual-input nonisolated DC–DC converter with vehicle-to-grid feature." *IEEE Journal of Emerging and Selected Topics in Power Electronics* 10.3 (2020): 3324-3336.

[19] Mazumder, Mondeep, and Sanjoy Debbarma. "EV charging stations with a provision of V2G and voltage support in a distribution network." *IEEE Systems Journal* 15.1 (2020): 662-671.

[20] Mishra, Debasish, Bhim Singh, and Bijaya Ketan Panigrahi. "Implementation of a robust PMAE algorithm to limit large gain variation in a fuel-cell integrated EV charging architecture." *IEEE Transactions on Energy Conversion* (2023).

[21] Shah, Vaibhav, and Saifullah Payami. "Integrated converter with g2v, v2g, and dc/v2v charging capabilities for switched reluctance motor drive-train based ev application." *IEEE Transactions on Industry Applications* (2023).

[22] Weearsinghe, Saranga, Duleepa J. Thrimawithana, and Udaya K. Madawala. "Modeling bidirectional contactless grid interfaces with a soft dc-link." *IEEE Transactions on Power Electronics* 30.7 (2014): 3528-3541.

[23] Monteiro, Vítor, J. G. Pinto, and João Luiz Afonso. "Operation modes for the electric vehicle in smart grids and smart homes: Present and proposed modes." *IEEE Transactions on Vehicular Technology* 65.3 (2015): 1007-1020.

54

[24] Kazemtarghi, Abed, Saikat Dey, and Ayan Mallik. "Optimal utilization of bidirectional EVs for grid frequency support in power systems." *IEEE Transactions on Power Delivery* 38.2 (2022): 998-1010.

[25] Zhang, Zhigang, Bin Liu, and Shaojian Song. "Power decoupling control for V2G/G2V/PV2G operation modes in single-phase PV/battery hybrid energy system with low DC-link capacitance." *IEEE Access* 9 (2021): 160975-160986.

[26] Kumar, Shailendra, Tapesh Upadhyay, and Om Hari Gupta. "Power quality improvement and signal conditioning of PV array and grid interfaced off-board charger for electric vehicles with V2G and G2V capabilities." *Chinese Journal of Electrical Engineering* (2023).

[27] Reddy, B. Mallikarjuna, and Paulson Samuel. "A comparative analysis of non-isolated bi-directional dc-dc converters." *2016 IEEE 1st International Conference on Power Electronics, Intelligent Control and Energy Systems (ICPEICES)*. IEEE, 2016.

[28] Gokul, Krishnan K., et al. "Design and control of non-isolated bidirectional DC-DC converter for energy storage application." *2017 2nd IEEE International Conference on Recent Trends in Electronics, Information & Communication Technology (RTEICT)*. IEEE, 2017.

[29] Ali, Abdelfatah, et al. "A comprehensive review on charging topologies and power electronic converter solutions for electric vehicles." *Journal of Modern Power Systems and Clean Energy* (2023).

[30] Rituraj, Gautam, Gautham Ram Chandra Mouli, and Pavol Bauer. "A comprehensive review on off-grid and hybrid charging systems for electric vehicles." *IEEE Open Journal of the Industrial Electronics Society* 3 (2022): 203-222.

[31] Metwly, Mohamed Y., et al. "A review of integrated on-board EV battery chargers: Advanced topologies, recent developments and optimal selection of FSCW slot/pole combination." *Ieee Access* 8 (2020): 85216-85242.

[32] Acharige, Sithara SG, et al. "Review of electric vehicle charging technologies, standards, architectures, and converter configurations." *IEEE Access* (2023).

[333] Safayatullah, Md, et al. "A comprehensive review of power converter topologies and control methods for electric vehicle fast charging applications." *IEEE Access* 10 (2022): 40753-40793.

[34] Sharma, Utsav, and Bhim Singh. "A Non-isolated Onboard Charger for Electric Vehicle." 2021 IEEE Transportation Electrification Conference & Expo (ITEC). IEEE, 2021.

[35] Zgheib, Rawad, Kamal Al-Haddad, and Innocent Kamwa. "V2G, G2V and active filter operation of a bidirectional battery charger for electric vehicles." *2016 IEEE International Conference on Industrial Technology (ICIT)*. IEEE, 2016.

[37] Cuk, Slobodan, and R. D. Middlebrook. "A new optimum topology switching DC-to-DC converter." *1977 IEEE Power Electronics Specialists Conference*. IEEE, 1977.

55

[38] Duran, E., Sidrach-de-Cardona, M., Galan, J., & Andujar, J. M. (2008, June). Comparative analysis of buck-boost converters used to obtain I–V characteristic curves of photovoltaic modules. In *2008 IEEE Power Electronics Specialists Conference* (pp. 2036-2042). IEEE.

[39] Seguel JL, Seleme SI Jr., Morais LMF. Comparative Study of Buck-Boost, SEPIC, Cuk and Zeta DC-DC Converters Using Different MPPT Methods for Photovoltaic Applications. *Energies*. 2022; 15(21):7936. https://doi.org/10.3390/en15217936

[40] Mittal, Sudhanshu, Alka Singh, and Prakash Chittora. "EV Control in G2V and V2G modes using SOGI Controller." 2022 IEEE 3rd Global Conference for Advancement in Technology (GCAT). IEEE, 2022.

[41] Pala, Sumanth, and S. P. Singh. "Design, modeling and implementation of Bi-directional buck and boost converter." *2012 IEEE 5th India International Conference on Power Electronics (IICPE)*. IEEE, 2012.

[42] B.Hauke, "Basic Calculation of a Buck Converter's Power Stage," Application report SLVA477b, Texas Instruments, Dec. 2011, Revised Aug. 2015.

[43] Hasaneen, B. M., and Adel A. Elbaset Mohammed. "Design and simulation of DC/DC boost converter." *2008 12th International Middle-East Power System Conference*. IEEE, 2008.

[44] Mokal, Bhushan P., and K. Vadirajacharya. "Extensive modeling of DC-DC Cuk converter operating in continuous conduction mode." *2017 International Conference on Circuit, Power and Computing Technologies (ICCPCT)*. IEEE, 2017.

[45] Kushwaha, Brijesh Kumar, and Anirudha Narain. "Controller design for Cuk converter using model order reduction." *2012 2nd International Conference on Power, Control and Embedded Systems*. IEEE, 2012.

# Conclusion and Future Scope

In this chapter conclusion from each chapter is summarized and also works of the future scope is discussed.

**Chapter 1**: This chapter discusses the importance of EV's. It also suggests how the battery can be used to support the grid. Later it mentions the importance of bidirectional converters in onboard chargers.

**Chapter 2**: This chapter presents a through literature survey on the existing DC-DC converters topology. It also mentions different configurations such as (single phase VSC, three phase VSC, and Multilevel inverter), single phase grid connected EV charging system, three phase grid connected solar PV and EV charging systems. This chapter also discusses literature survey regarding different control algorithms under various grid (single phase and three phase conditions). It discusses about the cuk converter and bidirectional buck and boost converter control.

**Chapter 3**: This chapter includes the detailed design aspects of different converter configurations. The design of bidirectional buck and boost converter. The design of bidirectional cuk converter. Operation of the converter in different switch condition is studied.

**Chapter 4**: In this chapter an on-board charger model is purposed. The designed system is modeled in MATLAB/Simulink. Control schemes for the grid and battery side converter is discussed. Performance in charging and discharging condition, under load variation and reference variations are studied for the bidirectional buck and boost converter and conclusions are made.

**Chapter 5**: This chapter discusses the behaviour of the bidirectional buck and boost dc-dc converter under distorted grid condition. The designed system is modeled in MATLAB/Simulink. Detailed design of GSC with SOGI PLL has been presented.

**Chapter 6**: This chapter presents the behaviour of the proposed model with the bidirectional dc-dc cuk converter. Control of the EV-Battery side converter under charging and discharging condition is presented. Simulation results are also presented and analyzed. Waveforms for buck and boost converter and cuk converter are compared with the cuk converter. Performance analysis under varying load condition and reference charging current is presented.

**Chapter 7**: This chapter discusses the performance of cuk converter with distorted

57

grid. The desired system is modelled in MATLAB/Simulink. Performance analysis under varying load condition is done for V2G and G2V operations. A comparison between both the bidirectional buck and boost and cuk converter done within this chapter.

## Scope of Future Work:

The research presented in this thesis on bidirectional onboard chargers with advanced control strategies represents a significant contribution to the field of electric vehicle power electronics. However, the rapidly evolving landscape of electric vehicle technology, smart grid integration, and power semiconductor advancements presents numerous opportunities for future research and development. This chapter outlines the potential directions for extending the current work, incorporating emerging technologies, and addressing the evolving challenges in electric vehicle charging systems.

## Model Predictive Control Implementation

While the current thesis employs PI control for DC-DC converter management and hysteresis control for AC-DC conversion, future developments should explore Model Predictive Control (MPC) strategies. MPC offers superior performance in handling the complex multi-objective optimization problems inherent in bidirectional charging systems. The integration of MPC with the existing SOGI PLL framework could enable more sophisticated grid synchronization under distorted conditions, building upon the harmonic rejection capabilities demonstrated in this thesis.

## Enhanced Grid Integration and Vehicle-to-Everything (V2X) Capabilities

The bidirectional nature of the converters studied in this thesis positions them ideally for Vehicle-to-Grid (V2G) and broader Vehicle-to-Everything (V2X) applications. Advanced V2X integration would enable the onboard charger to participate in virtual power plants, energy arbitrage, and emergency power provision during grid outages. The SOGI PLL system implemented for grid synchronization could be enhanced to support multiple grid codes and standards, enabling seamless operation across different electrical networks. Future research should investigate the integration of machine learning algorithms with the existing control framework to predict optimal charging and discharging schedules based on grid conditions, energy prices, and user behaviour patterns.

## Wireless and Dynamic Charging Integration

The future of onboard charging systems must accommodate wireless charging technologies, which eliminate physical connections and enable dynamic charging

58

during vehicle operation. The bidirectional converter topologies studied in this thesis could be adapted to support wireless power transfer, requiring modifications to the AC-DC conversion stage to handle the specific frequency and power characteristics of inductive charging systems.

This technology would require significant enhancements to the current control strategies, particularly in handling rapidly changing power levels and maintaining stable operation during varying coupling conditions. The hysteresis control method employed for the AC-DC converter could be modified to accommodate the variable frequency and power characteristics inherent in dynamic wireless charging systems.

### Intelligent Battery Management Integration

The CMC strategy employed in this thesis for battery charging current control represents a foundation for more sophisticated battery management systems. Future developments should integrate advanced battery modeling and state estimation algorithms to optimize charging and discharging profiles based on real-time battery condition assessment. This could include temperature-compensated charging algorithms, state-of-health monitoring, and predictive maintenance capabilities.

The bidirectional nature of the Cuk converter studied in this thesis makes it particularly suitable for implementing advanced battery balancing strategies. Future research could explore the use of the converter for active cell balancing during both charging and discharging operations, potentially extending battery life and improving overall system efficiency.

# List of Publications

- Verma, Aneeh, Alka Singh, and Rachana Garg. "Design and Performance Analysis of Cuk based Bidirectional EV Charger." *2024 3rd International Conference for Advancement in Technology (ICONAT)*. IEEE, 2024.